NACA

RESEARCH MEMORANDUM

THE EFFECT OF SURFACE ROUGHNESS ON THE PERFORMANCE OF A 23° CONICAL DIFFUSER AT SUBSONIC MACH NUMBERS

By Jerome Persh

Langley Aeronautical Laboratory
Langley Field, Va.

NATIONAL ADVISORY COMMITTEE
FOR AERONAUTICS

WASHINGTON

January 16, 1952

NATIONAL ADVISORY COMMITTEE FOR AERONAUTICS

RESEARCH MEMORANDUM

THE EFFECT OF SURFACE ROUGHNESS ON THE PERFORMANCE OF A 23° CONICAL DIFFUSER AT SUBSONIC MACH NUMBERS

By Jerome Persh

SUMMARY

An investigation was conducted to determine the effect of surface roughness on the performance of a 23° conical diffuser with a 2:1 ratio of exit to inlet area and with a constant-area tail pipe about $3\frac{1}{2}$ inlet diameters in length. The inlet-boundary-layer thickness was of the order of 5 percent of the inlet diameter. The air flows used in this investigation cover an inlet Mach number range from 0.10 to 0.64, corresponding to Reynolds numbers of 10^6 to 6×10^6 based on inlet diameter. The surface of the diffuser was coated with cork particles of a controlled size. Incremental bands of roughness were removed from the downstream edge after each series of pressure measurements were made and the variation of diffuser performance with percent of diffuser length roughened thereby determined.

The total-pressure losses increased considerably as the extent of the roughness was increased in the downstream direction from the smooth condition to about 48 percent of the diffuser length. The total-pressure-loss coefficient diminished smoothly from a maximum value when about 48 percent of the diffuser length was roughened to a value less than that measured at the tail-pipe exit for the smooth-surface diffuser, when the diffuser was almost fully roughened. The static-pressure recovery diminished as the extent of the roughness was increased from the smooth condition to the almost fully rough condition. The results indicated a progressive diminution of the static-pressure recovery and a continuous increase in the total-pressure losses as the inlet Mach number was increased for all configurations. In contrast to the fluctuating flow found in the same diffuser with smooth walls, the flow was steady for all roughness configurations. Flow separation was not found at the diffuser exit for any roughness configuration, although the same diffuser had substantial separated areas in the smooth condition.

INTRODUCTION

Most recent research has associated the inefficiency of wide-angle diffusers with the separation of the boundary layer. However, little is known of the mechanism of turbulence and its relationship to the characteristics of the boundary layer.

Experimentally it has been shown that the losses in wide-angle diffusers far exceed those anticipated from the skin friction alone. The additional losses, above those chargeable to skin friction, have been attributed to the unstable conditions accompanying boundary-layer separation.

From experience gained in pipe flow experiments, it would be expected that surface roughness would produce total-pressure losses proportionately higher than are found in the same smooth-surface diffuser. If, however, the surface roughness alters the turbulence structure of the boundary layer, as is the case for boundary-layer control devices such as vortex generators, a quite different result may be obtained. R. Jones and D. H. Williams (reference 1) found experimentally that when the back half of the upper surface of an R.A.F. 34 airfoil section was roughened, the values of maximum lift coefficient were substantially the same as found on the all-smooth-surface airfoil section, while the profile drag was appreciably diminished at high values of lift coefficient. This result indicated that roughening the airfoil surface in the region of adverse pressure gradient sufficiently changed the turbulent mixing process to produce the favorable result of reducing the profile drag.

With the advent of effective boundary-layer control devices which alter the turbulence structure of the boundary layer, it is of utmost importance that some insight be gained as to the factors which control this phenomenon. At the present time little is known about the mechanism which affects the ability of the turbulent boundary layer to transmit momentum. Inasmuch as the theoretical analysis of this problem appears remote, researchers must resort to experimental projects to determine the over-all effects rather than the underlying basic phenomena.

The present investigation was undertaken to obtain sufficient data to allow study of the effects of varying extents of surface roughness on the total-pressure losses and static-pressure-recovery characteristics of a 23° conical diffuser with a 2:1 ratio of exit to inlet area and with a constant-area tail pipe about $3\frac{1}{2}$ inlet diameters in length. The inlet-boundary-layer thickness was of the order of 5 percent of the inlet diameter. The data presented herein cover an inlet Mach number range from about 0.10 to 0.64 corresponding to Reynolds numbers of 10^6 to 6×10^6 based on inlet diameter. The surface of the diffuser was coated with

cork particles of a controlled size. Incremental bands of roughness were removed from the downstream edge after each series of pressure measurements were made so that the variation of diffuser performance with percent of diffuser length could be determined. For each configuration pressure measurements were made from which the total-pressure-loss coefficient, the static-pressure-recovery characteristics, and the longitudinal variation in static pressure were determined. Boundary-layer velocity profiles are presented at the diffuser inlet, the diffuser exit, and the tail-pipe exit.

SYMBOLS

p	static pressure
h	total pressure
M	Mach number
q_c	impact pressure $(h - p)$
Δh	weighted total-pressure loss from pressure surveys
Δp	wall static-pressure rise
Δq_c	change in impact pressure
r	radius
x	distance along longitudinal axis
y	perpendicular distance from diffuser wall
u	local velocity within boundary layer
u'	root-mean-square fluctuating velocity in axial direction
U	local velocity at edge of boundary layer
u/U	velocity ratio for incompressible flow $\left(\sqrt{\frac{h - p_{wall}}{h_{max} - p_{wall}}}\right)$
W	weight flow
δ	boundary-layer thickness at $0.95\frac{u}{U}$

[redacted]

δ^* boundary-layer displacement thickness for incompressible flow $\left(\delta \int_0^{1.0} \left(1 - \frac{u}{U}\right) d\left(\frac{y}{\delta}\right)\right)$

θ boundary-layer momentum thickness for incompressible flow $\left(\delta \int_0^{1.0} \frac{u}{U}\left(1 - \frac{u}{U}\right) d\left(\frac{y}{\delta}\right)\right)$

H boundary-layer shape parameter for incompressible flow $\left(H = \frac{\delta^*}{\theta}\right)$

$\tau_0/2q$ skin-friction coefficient

Diffuser performance parameters:

$\frac{\Delta h}{q_{c_1}}$ total-pressure-loss coefficient

$\frac{\Delta p}{\Delta p_{ideal}}$ diffuser effectiveness

Subscripts:

0	reference conditions	to conform with stations designated in reference 2
1	diffuser inlet conditions	
6	diffuser exit conditions	
7	tail-pipe exit conditions	

APPARATUS AND TESTS

General arrangement.- The apparatus used for this investigation is shown in figure 1. A part of the investigation reported in reference 2 was made by using this apparatus. The duct system consists of a 23° conical diffuser with a 2:1 ratio of exit to inlet area joined to a 21-inch cylindrical approach tube approximately $4\frac{1}{2}$ inlet diameters in length.

The junction between the approach tube and diffuser was formed as a circular arc of $5\frac{3}{16}$-inch radius, tangent to both the inlet cylinder and diffuser cone. A discharge tail pipe of approximately $3\frac{1}{2}$ inlet diameters in length was attached to the diffuser exit. A photograph of the duct arrangement is shown in figure 2. The exit-pressure-loss rakes indicated in the photograph were not in place for this investigation.

Roughness particle size.- The wall skin-friction coefficient $\tau_0/2q$ was the factor by which the size of the particles used to produce the surface roughness was selected. For this investigation the average skin-friction coefficient was to be approximately three times that for the smooth surface. The average skin-friction coefficient for the smooth-surface diffuser is of the order of 0.0012 over the range of Reynolds numbers investigated. To produce a skin-friction coefficient approximately three times the smooth-surface value, it was found, by using the data of J. Nikuradse (reference 3), that it was necessary to use particles of about 0.100 inch in diameter. By using cork particles that would pass through a standard 8-mesh-to-the-inch screen but be retained on a standard 14-mesh screen, it was possible to approximate the desired particle size. The mean diameter of the particles used is 0.098 inch, and the data of reference 3 indicate that the average skin-friction coefficient for roughness made up of these particles is 0.00350. No Reynolds number effect on the value of $\tau_0/2q$ was considered because the curve given in reference 3 of $\tau_0/2q$ against Reynolds number indicates little variation in $\tau_0/2q$ with Reynolds number over the range of Reynolds numbers encountered in this investigation.

The cork particles were cemented uniformly about the entire interior surface of the diffuser between the points indicated in figure 1. To avoid a ledge effect as the flow enters the diffuser, the leading edge of the roughness was placed about $\frac{1}{2}$ inch downstream of the midpoint of the junction arc, and buffed and smoothly faired from the leading edge to a point about 2 inches downstream. A photograph of the diffuser with the roughness installed is shown in figure 3.

Description of configurations.- The first series of pressure measurements were made with 97.5 percent of the diffuser length roughened. This condition is designated as configuration I. Incremental bands of cork were removed from the downstream edge after each series of pressure measurements were made so that the variation of the diffuser performance with percent of diffuser length roughened could be determined. After each band of roughness was removed, the surface of the diffuser downstream of the trailing edge of the roughness was carefully sanded to insure a smooth surface. Succeeding configurations were tested with 70 percent,

47.7 percent, and 4.70 percent of the diffuser length roughened. These conditions are designated as configurations II, III, and IV, respectively.

Instrumentation.- A series of static-pressure orifices were installed along one generatrix of the diffuser and tail pipe to record longitudinal pressure distributions. At stations 1, 6, and 7 (fig. 1), wall static-pressure measurements were made at six equally distributed positions. All static-pressure orifices were connected to a multitube manometer and pressures recorded photographically. Total- and static-pressure surveys were made at stations 1, 6, and 7 for configurations I, II, and III by using a remotely controlled electrically driven device which could extend the pressure tube across the stream in accurate increments of distance. A diagram of the instrument used for pressure surveys is shown in figure 1. With this pressure tube, it was possible to measure the total pressure approximately 0.020 inch from the wall.

To determine whether the flow was symmetrical at the diffuser exit, a series of pitot-static surveys were made in four transverse planes, by using a pitot-static pressure rake which extended across the stream from wall to wall and could be rotated through 360° during the course of the test. A photograph of this instrument installed in the tail pipe is shown as figure 4. The rotating rake was installed after tail-pipe pressure measurements were made for configuration III and was left in place for configuration IV. Because of the presence of the rotating rake assembly it was not possible to make any tail-pipe pressure measurements for configuration IV.

Testing procedure.- For each configuration the following series of pressure measurements were made over the inlet Mach number range in the following sequence:

(1) Measurements were made of the longitudinal wall static-pressure distribution.

(2) For configurations I, II, and III, total- and static-pressure surveys were made at stations 7, 6, and 1, in that order, by using the exploring tube. For configuration IV, total and static surveys were made at station 6 by use of the rotating rake and inlet surveys were made by use of the exploring tube.

The intake duct arrangement used for configurations III and IV was such as to limit the inlet velocity obtainable with the blowers available to a value less than that for configurations I and II. Therefore, for configurations III and IV, it was not possible to cover the complete range of air flows investigated for configurations I and II.

[redacted]

METHODS AND ANALYSIS

Computational methods.- Since it was impossible to record simultaneous upstream and downstream pressure measurements because the inlet duct and the diffuser must be free of all obstructions upstream of any station at which pressure measurements are being made, it was necessary to use a correlating parameter for the computation of the performance coefficients. All pressure measurements were referred to the upstream total pressure and the inlet pressure ratio p_1/h_0 was used as the correlating parameter for calculating all performance coefficients.

Calculation of performance parameters.- The volume-weighted mean loss in total pressure from the reference station 0 to the station in question was computed in the following manner:

$$\Delta h_{0,x} = \overline{h_0 - h_x} = \frac{\int_0^r u(h_0 - h_x)y \, dy}{\int_0^r uy \, dy} \tag{1}$$

The mean loss in total pressure was computed for both the diffuser and the diffuser and tail pipe by using the following relations:

Diffuser:

$$\Delta h_{1,6} = \overline{(h_0 - h_6)} - \overline{(h_0 - h_1)} \tag{2}$$

Diffuser and tail pipe:

$$\Delta h_{1,7} = \overline{(h_0 - h_7)} - \overline{(h_0 - h_1)} \tag{3}$$

The rise in static pressure was computed as the difference between the arithmetic mean of the six wall static-pressure measurements at station 1, and the arithmetic mean of the wall static-pressure measurements at station 6 and station 7. The theoretical gain in static pressure was computed by assuming frictionless one-dimensional flow.

Diffuser performance parameters.- In order to provide a basis for comparison of the results of the present investigation with those of reference 2, the same performance parameters as presented therein are used in the current analysis. The coefficients are given as follows:

(1) The total-pressure-loss coefficient, defined as the mean loss in total pressure between stations divided by the inlet impact pressure:

$$\text{Total-pressure-loss coefficient} = \frac{\Delta h}{q_{c_1}}$$

(2) The diffuser effectiveness, defined as the actual gain in static pressure between stations divided by the gain in static pressure possible with frictionless flow:

$$\text{Diffuser effectiveness} = \frac{\Delta p}{\Delta p_{ideal}}$$

RESULTS AND DISCUSSION

In the current investigation only the thicker inlet-boundary-layer condition of reference 2 was used; for both cases the inlet-boundary-layer thickness is of the order of 5 percent of the inlet diameter. All comparisons between the data presented herein and those of reference 2 are made for this inlet-boundary-layer thickness.

Performance curves are plotted against the inlet pressure ratio p_1/h_0 as in reference 2. A curve of inlet flow characteristics is presented in figure 5, which gives the variation of inlet Mach number with inlet pressure ratio. This correlating parameter was chosen as an approximate index of inlet Mach number and flow rate.

Flow in roughened diffuser.- One of the primary purposes of the present investigation was to give detailed attention to the flow in the diffuser. In contrast to the flow in the smooth-surface diffuser which shifted position from time to time and lacked axial symmetry, the flow in the roughened diffuser was steady and had approximately symmetrical velocity profiles at the diffuser exit for all configurations investigated. Velocity profiles measured at station 6 with the rotating pressure rake (fig. 4) are shown in figure 6 for configurations III and IV. Tuft surveys indicated that the extensive areas of reversed flow found in the smooth-surface diffuser were absent in the roughened diffuser although very low wall velocities were noted in the downstream

regions. Pressure surveys at the diffuser exit confirmed this observation. Unlike the smooth-surface diffuser, it was possible to make detailed pressure surveys at the end of the conical expansion, because of the steadiness of the flow, and to determine the performance parameters at the diffuser exit.

Pressure Survey Results

As pointed out in reference 2, difficulty in making pressure surveys at the diffuser exit made it impractical in that investigation to present values of $\Delta h/q_{c_1}$ at that point. In the present investigation, however, the steady flow at station 6 made it possible to make detailed pressure surveys at that point and values of $\Delta h/q_{c_1}$ are presented at both station 6 and station 7. The diffuser effectiveness is the only performance parameter for which a comparison can be made at station 6, between the smooth-surface diffuser results of reference 2 and the roughened diffuser.

Weight-flow check.- The weight flow was calculated for each configuration at each measuring station to determine whether true mean values of total and static pressure are recorded by the pressure tubes used in this investigation. The results of this check are shown in figure 7, in which the weight flow is plotted as a function of the inlet pressure ratio, for all configurations at each of the measuring stations. For all configurations (figs. 7(a) to 7(d)) the weight flows calculated from pitot-tube measurements at both the diffuser exit and the tail-pipe exit are slightly higher than the weight flows calculated from pitot-tube measurements at the inlet over the entire speed range. This apparent inconsistency may partially be traced to the behavior of a total-pressure tube in an air stream containing axial fluctuating velocities. As pointed out in reference 4 the total pressure recorded by a pitot tube in such an air stream may be expressed by the following approximate relation:

$$h = p + \frac{1}{2}\rho\left(u^2 + \overline{u'^2}\right) \tag{4}$$

Because $\overline{u'^2}$ is always positive, the apparent total pressure is always greater than the mean total pressure by the amount of $\frac{1}{2}\rho\left(\overline{u'^2}\right)$. Since the axial turbulent fluctuating velocities do not contribute to the weight flow, it can be seen that the weight flow calculated from total-pressure measurements obtained by the pitot-tube method in a stream with axial fluctuating velocities will always be higher than the actual weight flow.

Total-pressure-loss coefficient.- The variation of $\Delta h/q_{c_1}$ with inlet pressure ratio is shown in figure 8(a) at the diffuser exit, and figure 8(b) at the tail-pipe exit, for all configurations. At both measuring stations, the values of $\Delta h/q_{c_1}$ increased with increasing inlet velocity for all configurations. At station 6, (fig. 8(a)) the rate of increase of $\Delta h/q_{c_1}$ with increasing inlet velocity is approximately the same for all configurations. It should be noted that the values of $\Delta h/q_{c_1}$ for successive configurations I, II, and III are in an increasing order, whereas the values of $\Delta h/q_{c_1}$ for configuration IV lie between those of configurations I and II. At the tail-pipe exit, (fig. 8(b)) the rate of increase of the values of $\Delta h/q_{c_1}$ for configuration I, with increasing inlet velocity, is approximately the same as that of the data of reference 2. However, the rate of increase of the values of $\Delta h/q_{c_1}$ with increasing inlet velocity for configurations II and III is somewhat less than that for either configuration I or the smooth-surface diffuser (reference 2).

It should be noted that the calculated values of $\Delta h/q_{c_1}$ for all configurations are slightly lower than the true values. As was shown in the preceding section, the values of total pressure recorded by the pitot tubes are higher than the actual values and therefore when integrated across the stream, result in lower total-pressure-loss coefficients. However, the magnitude of this error cannot be ascertained because the distribution of $\frac{1}{2}\rho\overline{u'^2}$ across the stream is not known. However, since this effect is nearly the same for all configurations at any single velocity over the speed range, only the values of $\Delta h/q_{c_1}$, not the shape of the curves, plotted in figure 6 will be slightly affected.

Figure 9 shows the variation of $\Delta h/q_{c_1}$ with percent of diffuser length roughened for both measuring stations at a constant inlet pressure ratio of 0.90. At both the diffuser exit and tail-pipe exit the total-pressure-loss coefficient increased considerably as the extent of the roughness increased from the smooth condition to the 47.7 percent of the diffuser length roughened condition. Values of $\Delta h/q_{c_1}$ at both station 6 and station 7 diminished smoothly from the value when 47.7 percent of the diffuser length was roughened to values which are less than that for the smooth-surface diffuser at the tail-pipe exit, when the diffuser was almost fully roughened. This result agrees qualitatively with the results of experiments by R. Jones and D. H. Williams (reference 1) in which it was found that when the entire back half of the upper surface (adverse pressure gradient region) of an R.A.F. 34 airfoil section was roughened, the profile drag was appreciably diminished at high values of lift coefficient.

From experiments on rough plates, Tillman (reference 4) found that roughness increases the ability of the turbulent boundary layer to transmit momentum. The results of the current experiment confirm Tillmann's finding to a certain extent, and indicate that this effect causes the values of $\Delta h/q_{c_1}$ obtained with the diffuser almost fully roughened, to fall below those of the smooth-surface diffuser in spite of the increased skin friction.

Diffuser effectiveness.- The variation of the diffuser effectiveness with inlet pressure ratio is shown in figure 10 for both the diffuser exit and the tail-pipe exit, for all configurations. For comparison purposes the curves of $\Delta p/\Delta p_{ideal}$ from reference 2 have been added. In figure 10(a), which shows the diffuser effectiveness measured at station 6, the values of $\Delta p/\Delta p_{ideal}$ for configurations I and II diminish with increasing air flow at a slightly greater rate than do the values of $\Delta p/\Delta p_{ideal}$ for the smooth-surface diffuser and are approximately 87 percent of the smooth-surface values over the range of air flows investigated. At the lower air flows the values of $\Delta p/\Delta p_{ideal}$ for configurations III and IV are appreciably higher than those for the smooth-surface diffuser. However, the values of $\Delta p/\Delta p_{ideal}$ diminish rapidly with increasing air flow until they appear to fall on the smooth-surface curve at about $\frac{p_1}{h_0} = 0.90$. The values of $\Delta p/\Delta p_{ideal}$ measured at the tail-pipe exit are shown in figure 10(b) for all configurations. In this case the values of $\Delta p/\Delta p_{ideal}$ for all configurations and for values of p_1/h_0 less than 0.94, diminish with increasing air flow at approximately the same rate as the smooth-surface diffuser values and are approximately 95 percent of those obtained in the smooth diffuser.

Figure 11 shows the variation of $\Delta p/\Delta p_{ideal}$, at both measuring stations, with percent of diffuser length roughened at a constant inlet pressure ratio of 0.90. The curves shown in figure 11 indicate that the values of $\Delta p/\Delta p_{ideal}$ at both the diffuser exit and the tail-pipe exit diminish smoothly with increasing extent of roughness. These curves indicate that the static-pressure-recovery characteristics of the diffuser are far less affected by the roughness than are total-pressure losses discussed in the previous section.

Longitudinal variation in static pressure.- The variation in static pressure along the wall of the diffuser is shown in figures 12 to 15, each figure representing a different configuration. This variation is shown for a number of different inlet Mach numbers identified by the values of inlet pressure ratio p_1/h_0. On each figure a section of the diffuser wall is shown with the extent of the roughness indicated.

To determine whether the roughness influenced the wall static-pressure measurements, a check was made by using an exploring tube set several inches from the wall at a number of different longitudinal positions. For the axial positions investigated it was found that the static pressure measured through orifices set in the roughness was very close to that measured several inches from the wall in the same transverse plane. This agreement is attributed to the extremely low boundary-layer velocity close to the ridges of the roughness particles. On the basis of the check made it was assumed that the static pressure measured through the orifices set on the diffuser wall are true values and these are plotted in figures 12 to 15. It should be noted that no discontinuity appears in the curves of static-pressure distributions (figs. 12 to 15) at the trailing edge of the roughness.

Figure 16 shows the longitudinal static-pressure distribution in the diffuser and tail pipe for several values of inlet pressure ratio p_1/h_0. The curves of figure 16 have been derived from cross plots of the data given in figures 12 to 15 in order to permit superimposing static-pressure profiles for all configurations at common values of inlet pressure ratio p_1/h_0. The longitudinal variation in static pressure for the smooth-surface diffuser (reference 2) has been added for comparison purposes. The static-pressure distributions in the tail pipe of configuration IV were not measured because of the presence of the large pressure rake installed at the diffuser exit. It should be noted that the static pressure continues to rise as the distance along the tail pipe increases for all configurations shown. This condition is due to the natural process of the distorted velocity profile at the diffuser exit reverting to a profile characteristic of fully developed pipe flow.

Boundary-layer profiles.- The velocity profiles computed from pressure measurements made at station 1 are shown in figure 17 for all configurations and velocity profiles at stations 6 and 7 are shown in figures 18, 19, and 20 for configurations I, II, and III, respectively. No boundary-layer profiles were measured for configuration IV. Although it is not apparent because of the scale of figures 17 to 20, the data point indicated at $y = 0$ is approximately 0.020 inch from the wall. The boundary-layer parameters δ, θ, δ^*, and H given for each of the profiles presented were computed by using two-dimensional definitions; compressibility corrections were not included.

It is of particular interest to compare the diffuser exit (station 6) velocity profiles measured in the smooth-surface diffuser (reference 2) and those measured in the roughened diffuser. For this comparison, station 6 velocity profiles have been plotted in figure 21 for each of the configurations investigated at an approximately constant inlet pressure ratio of 0.90 along with a station 6 velocity profile measured in the smooth-surface diffuser (reference 2) at the same inlet pressure

ratio p_1/h_0. Figure 21 indicates that the flow separation in the smooth-surface diffuser at station 6 is absent for configurations I, II, and III. Although detailed pressure surveys were not made for configuration IV, the rotating rake pressure measurements made at station 6 did not indicate any areas of flow separation. These results when considered with the wand tuft surveys made along the length of the diffuser indicate that the roughness suppresses the flow separation that was found in the smooth-surface diffuser. In accordance with results previously discussed in the section entitled "Loss Coefficient," it is apparent that the over-all boundary-layer thickness δ is less for configuration I than the other roughness configurations as well as the smooth-surface configuration.

The velocity profiles in the tail pipe (station 7) shown in figures 18(b), 19(b), and 20(b) for configurations I, II, and III, respectively, all show evidence of the distorted velocity profiles measured at station 6 (figs. 18(a), 19(a), and 20(a)) which indicates that fully developed pipe flow is not yet established in the length of tail pipe provided. This observation is supported by the data of Peters (reference 5) which show that the length of tail pipe needed to attain fully developed pipe flow is more than twice that used in the current investigation.

CONCLUSIONS

From the current investigation regarding the effect of surface roughness on the performance of a 23° conical diffuser with a 2:1 ratio of exit to inlet area and with a constant-area tail pipe $3\frac{1}{2}$ inlet diameters in length, with an inlet-boundary-layer thickness approximately 5 percent of the inlet diameter, the following conclusions are drawn:

1. The total-pressure-loss coefficients measured at the diffuser exit and the tail-pipe exit increased considerably as the extent of the roughness was increased in the downstream direction from the smooth condition to about 48 percent of the diffuser length. The total-pressure-loss coefficients at both measuring stations diminished smoothly from a maximum value when about 48 percent of the diffuser length was roughened to a value measurably less than that measured at the tail-pipe exit for the smooth-surface diffuser, when the diffuser was almost fully roughened.

2. The static-pressure recovery diminished as the extent of the roughness was increased from the smooth condition to the almost fully rough condition, at both the diffuser exit and the tail-pipe exit.

3. For all configurations investigated, the total-pressure losses increased continuously and the static-pressure recovery progressively

diminished as the inlet Mach number was increased. For all roughness configurations investigated the rate of increase of the total-pressure-loss coefficient with increasing Mach number, at both downstream measuring stations, is essentially the same as that found in the smooth-surface diffuser at the tail-pipe exit.

4. For all roughness configurations investigated the flow in the diffuser was extremely steady over the entire speed range.

5. No evidence of separation was found within the diffuser for any of the roughness configurations investigated. Reversed flow was not detected at the measurement point closest to the wall for any of the roughness configurations.

Langley Aeronautical Laboratory
National Advisory Committee for Aeronautics
Langley Field, Va.

REFERENCES

1. Jones, R., and Williams, D. H.: The Effect of Surface Roughness on the Characteristics of the Aerofoils N.A.C.A. 0012 and R.A.F. 34. R. & M. No. 1708, British A.R.C., 1936.

2. Persh, Jerome: The Effect of the Inlet Mach Number and Inlet-Boundary-Layer Thickness on the Performance of a 23° Conical-Diffuser - Tail-Pipe Combination. NACA RM L9K10, 1950.

3. Nikuradse, Johann: Laws of Flow in Rough Pipes. NACA TM 1292, 1950.

4. Tillmann, W.: Investigations of Some Particularities of Turbulent Boundary Layers on Plates. Reps. and Translations No. 45, British M.A.P. Völkenrode, March 15, 1946. (Issued by Joint Intelligence Objectives Agency with File No. B.I.G.S.-19.)

5. Peters, H.: Conversion of Energy in Cross-Sectional Divergences under Different Conditions of Inflow. NACA TM 737, 1934.

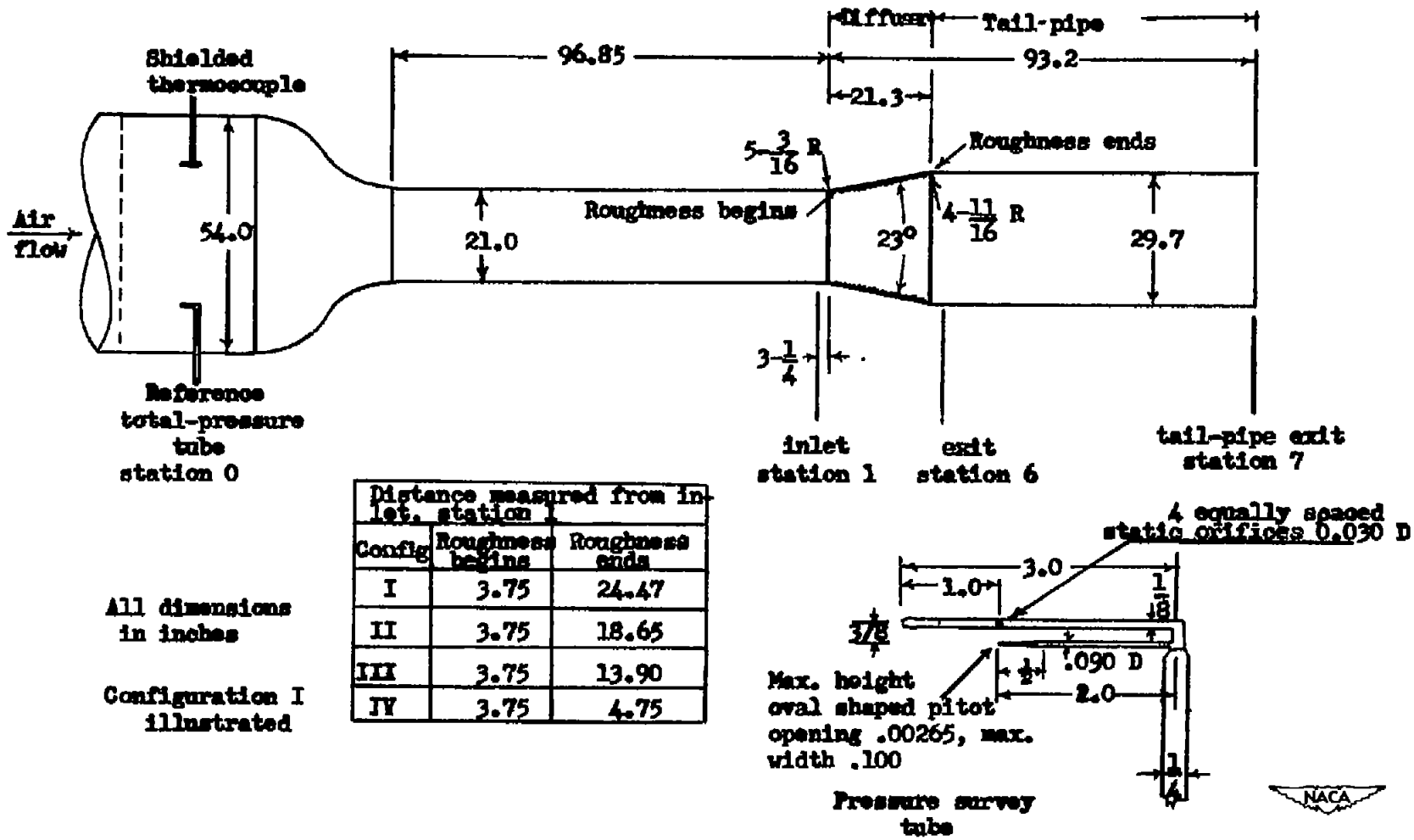

Config	Distance measured from inlet, station 1: Roughness begins	Roughness ends
I	3.75	24.47
II	3.75	18.65
III	3.75	13.90
IV	3.75	4.75

Figure 1.- General arrangement of test apparatus and instrumentation.

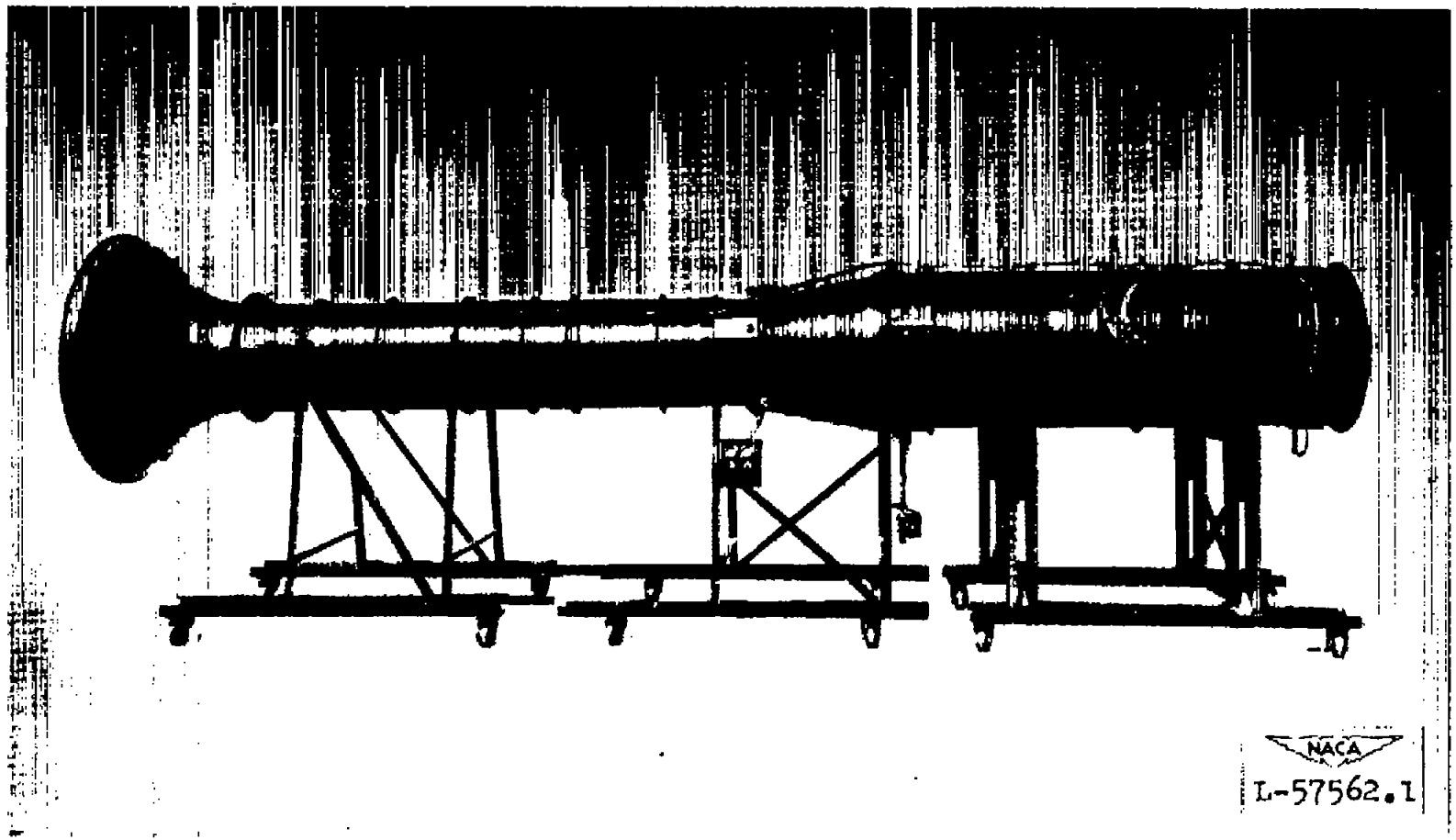

Figure 2.- Photograph of test setup showing inlet pipe, diffuser, and tail pipe.

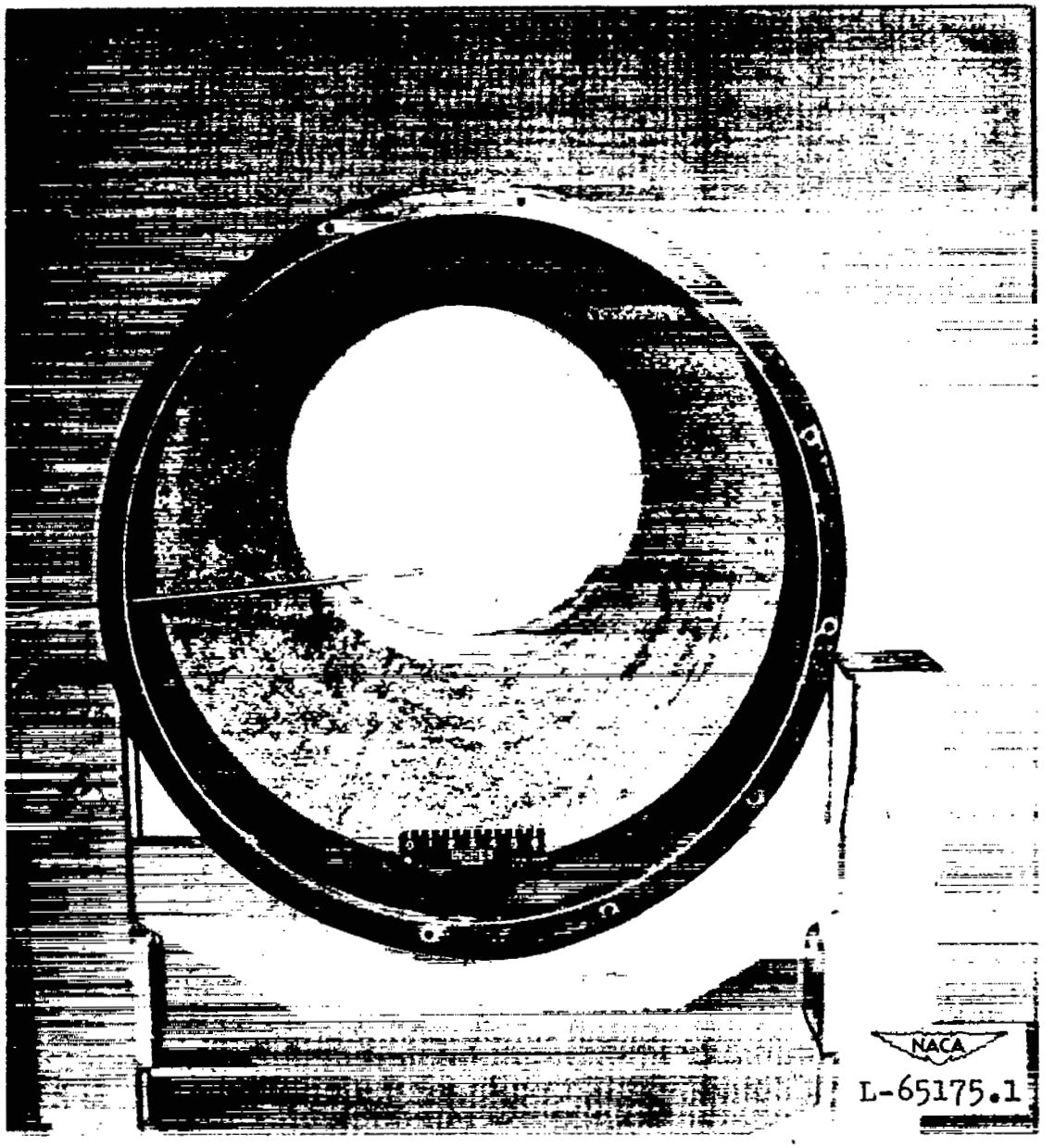

Figure 3.- Photograph of diffuser with roughness installed.

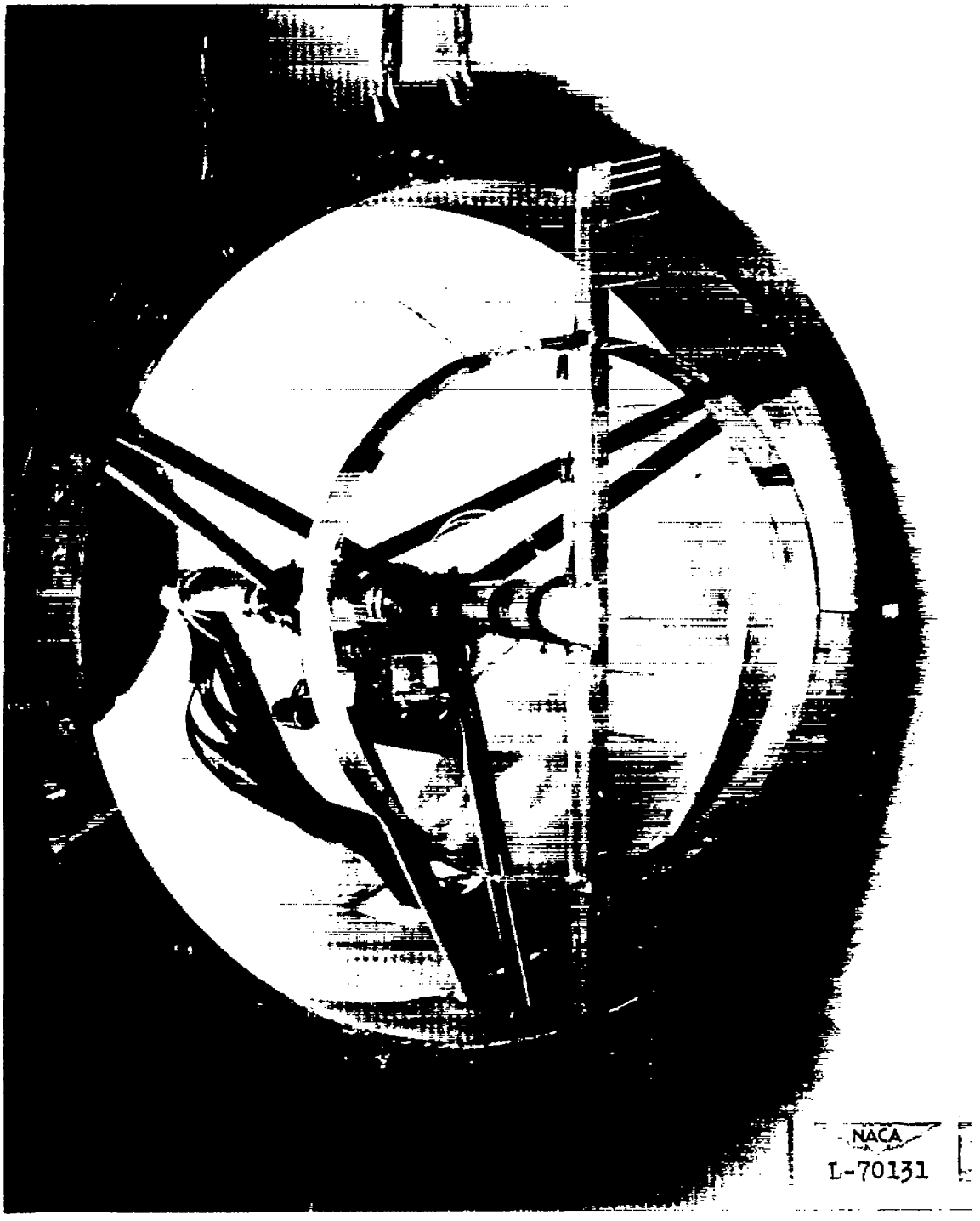

Figure 4.- Photograph of diffuser-exit pressure tube survey rake with rotating mechanism.

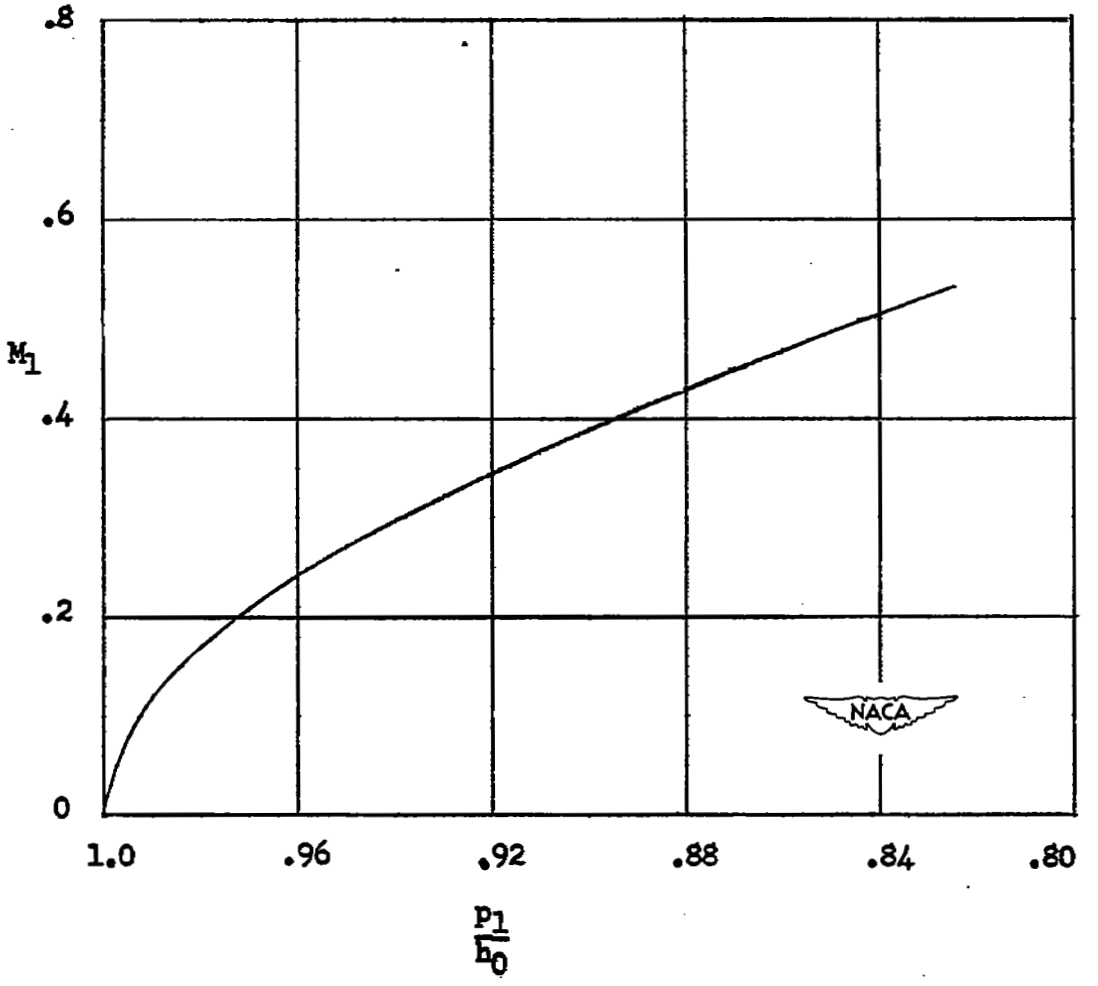

Figure 5.- Variation of inlet Mach number with inlet pressure ratio.

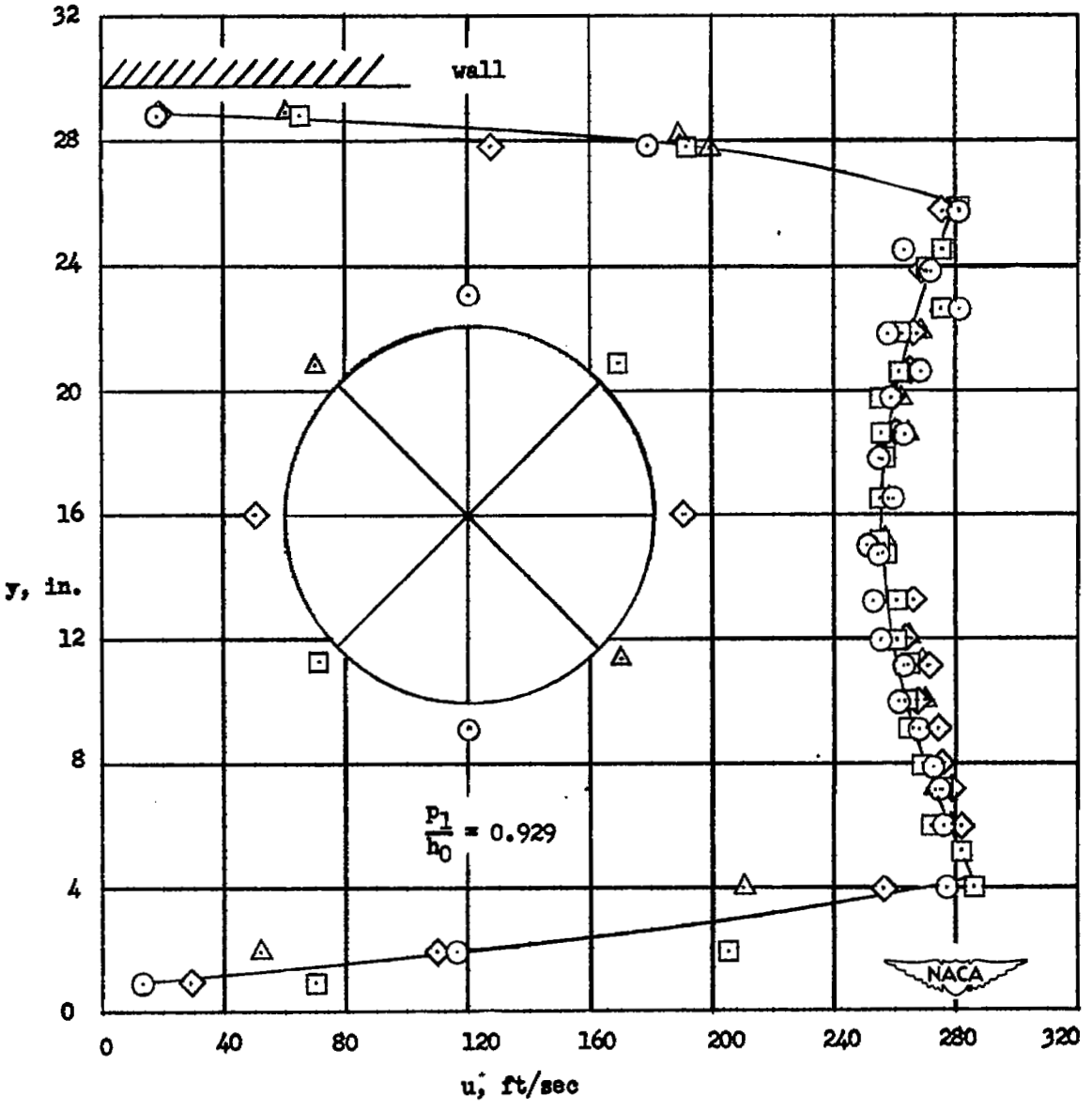

(a) Configuration III.

Figure 6.- Velocity profile at station 6.

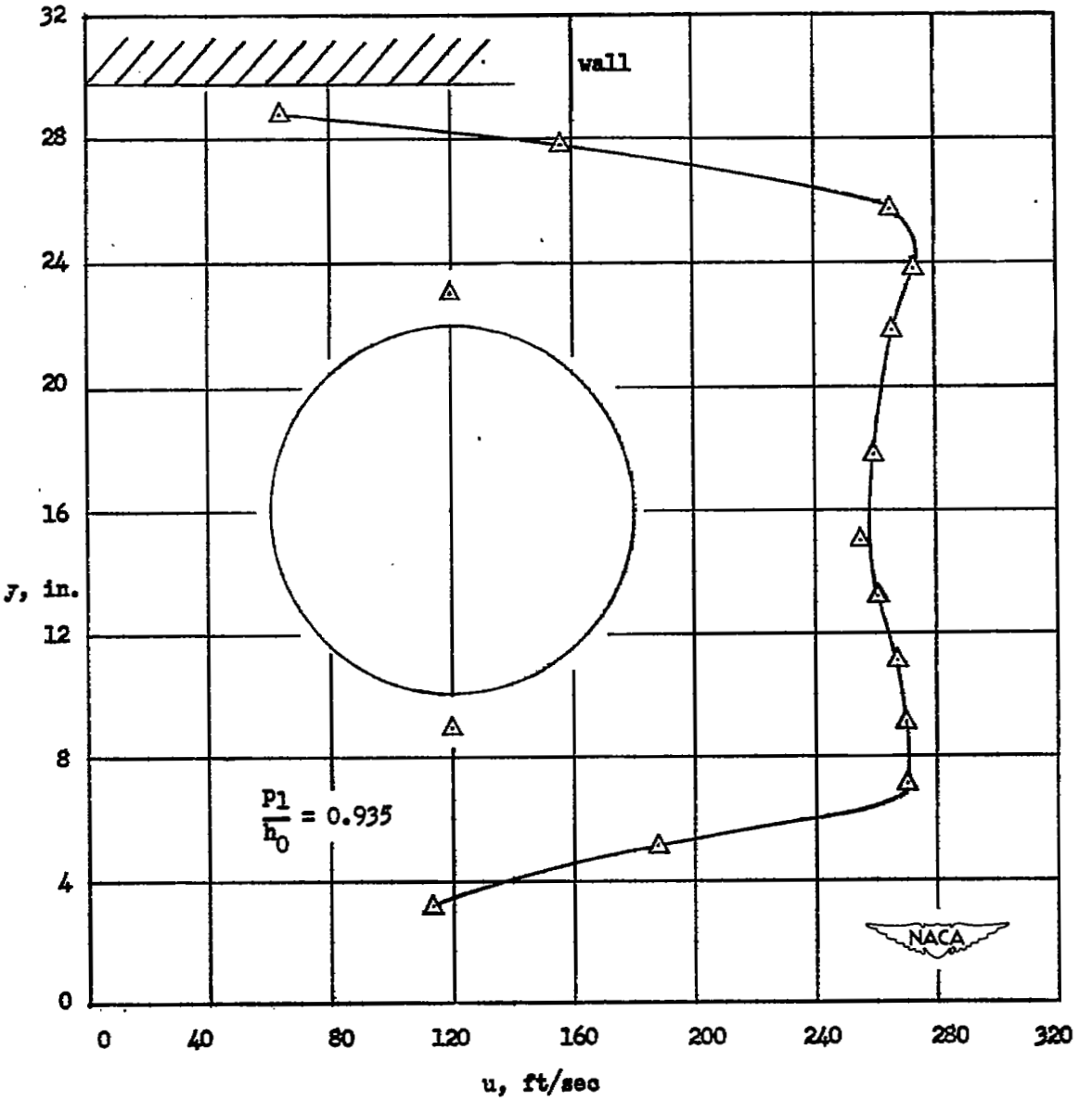

(b) Configuration IV.

Figure 6.- Concluded.

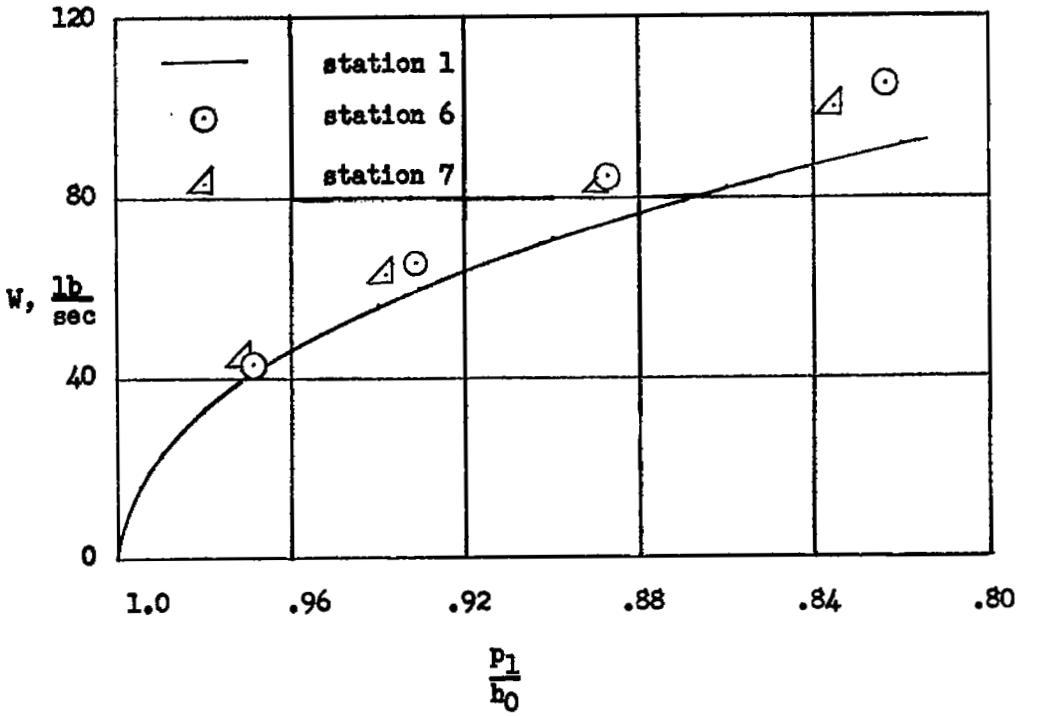

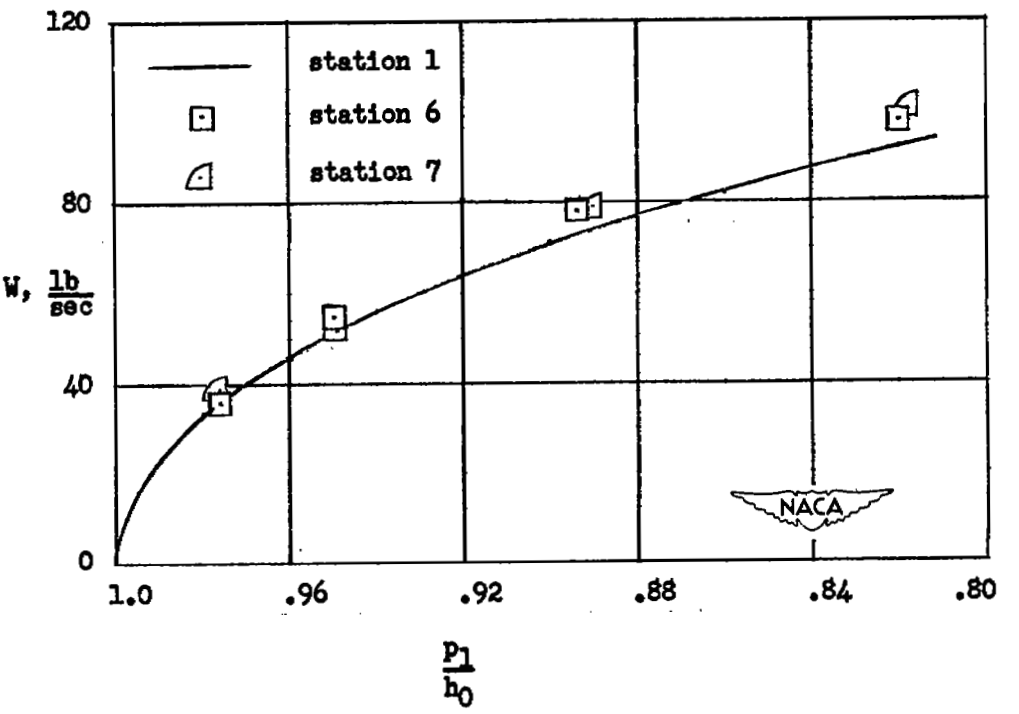

(a) Configurations I and II.

Figure 7.- Variation of weight flow with inlet pressure ratio.

[redacted]

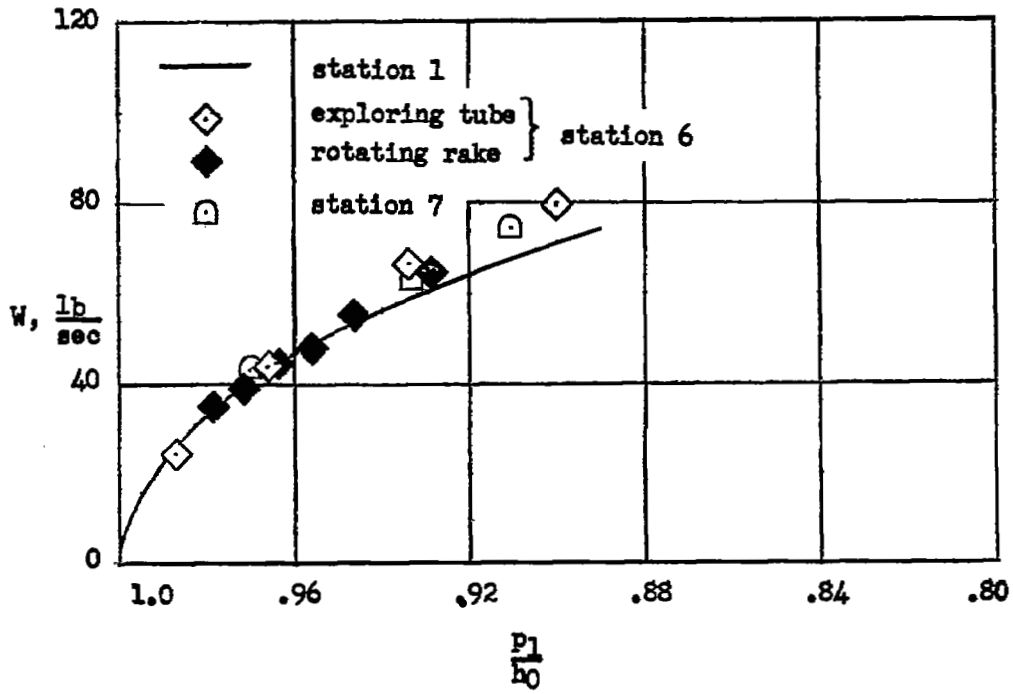

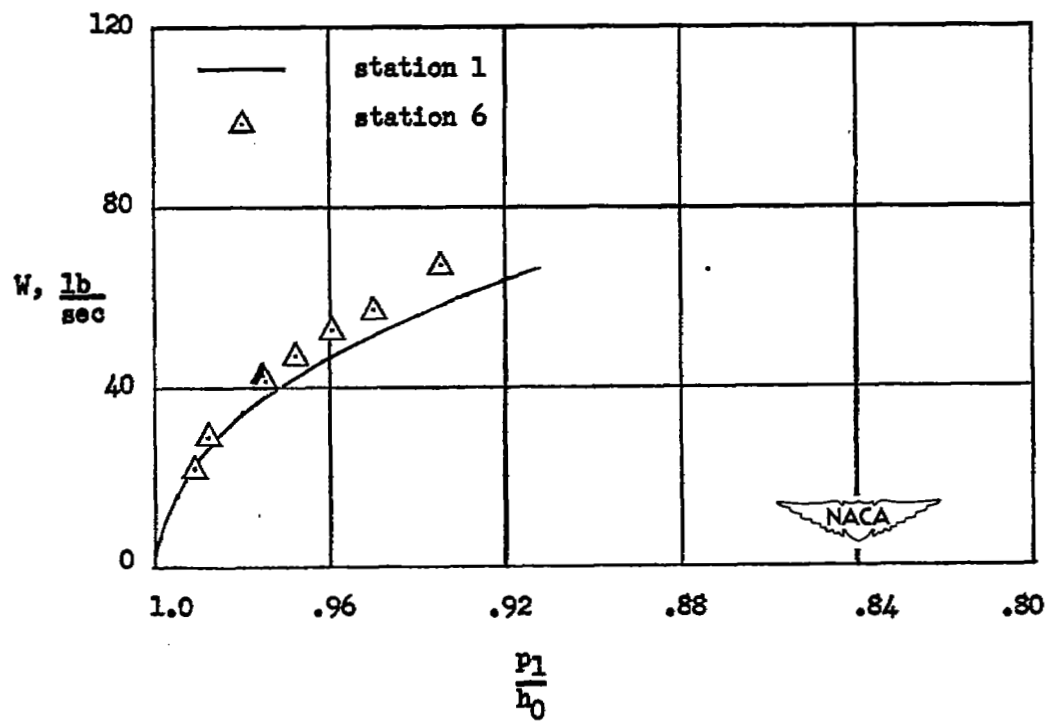

(b) Configurations III and IV.

Figure 7.- Concluded.

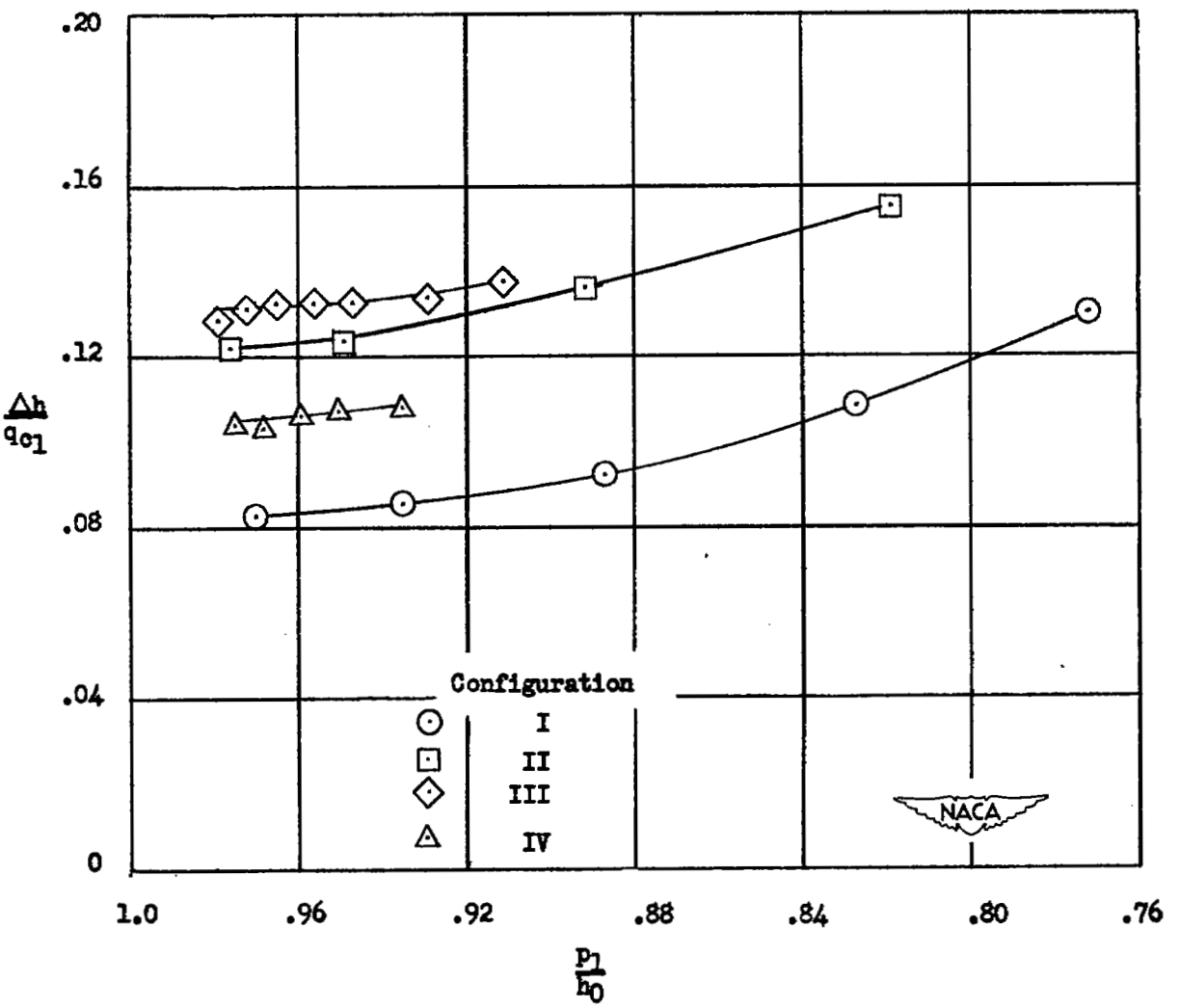

(a) Diffuser exit, station 6.

Figure 8.- Variation of total-pressure-loss coefficient with inlet pressure ratio.

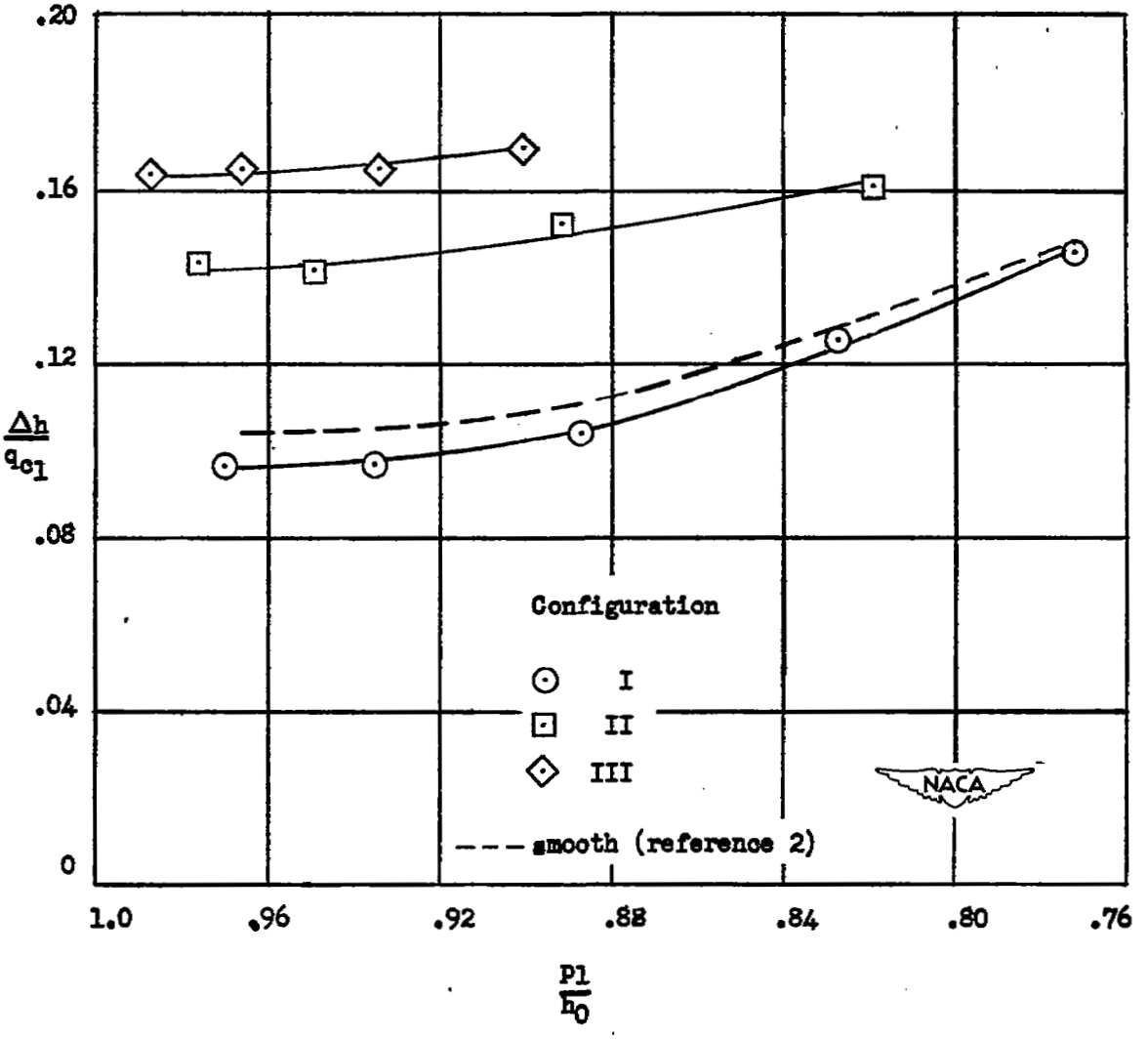

(b) Tail-pipe exit, station 7.

Figure 8.- Concluded.

[redacted]

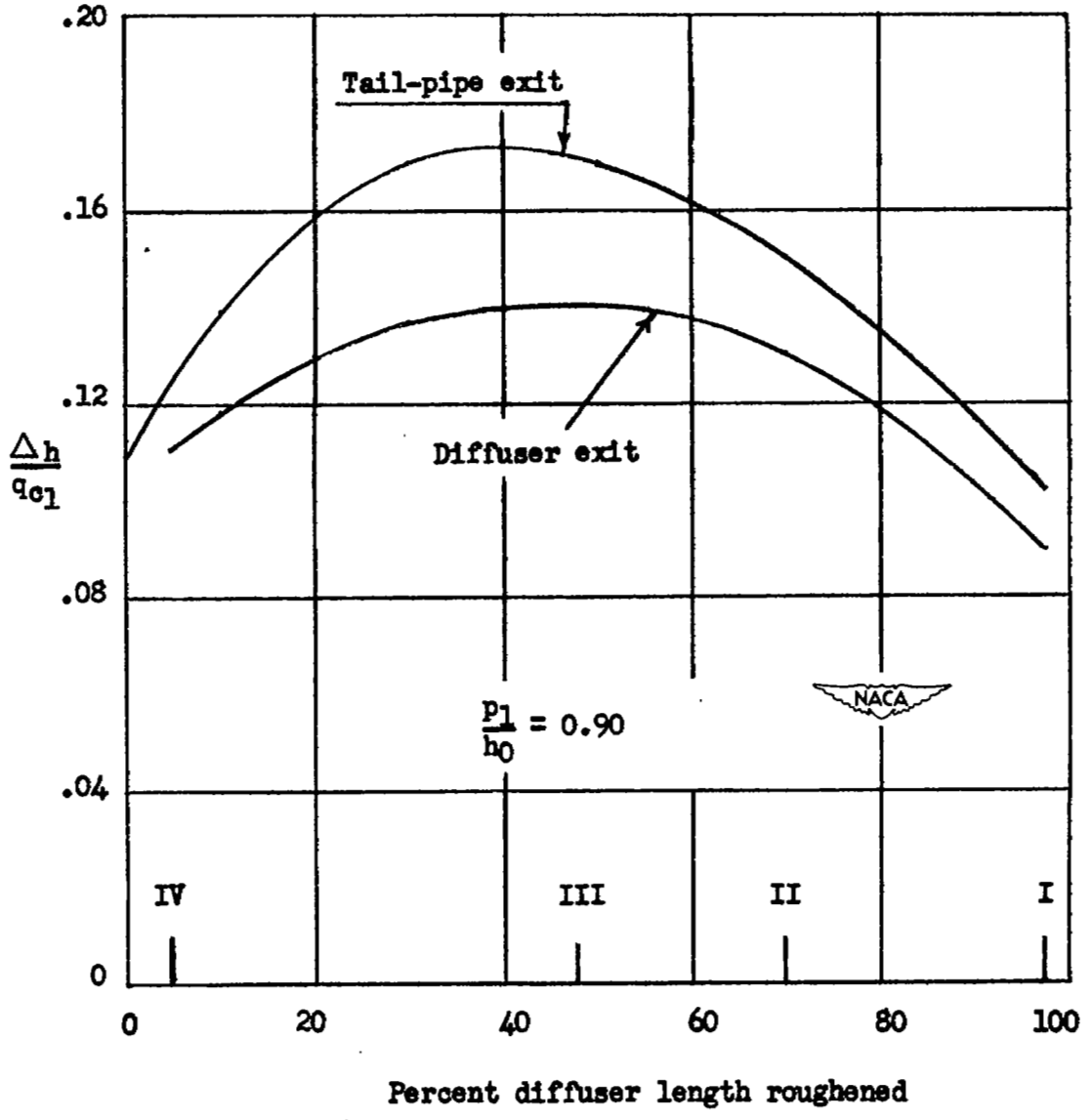

Figure 9.- Variation of total-pressure-loss coefficient with percent of diffuser length roughened.

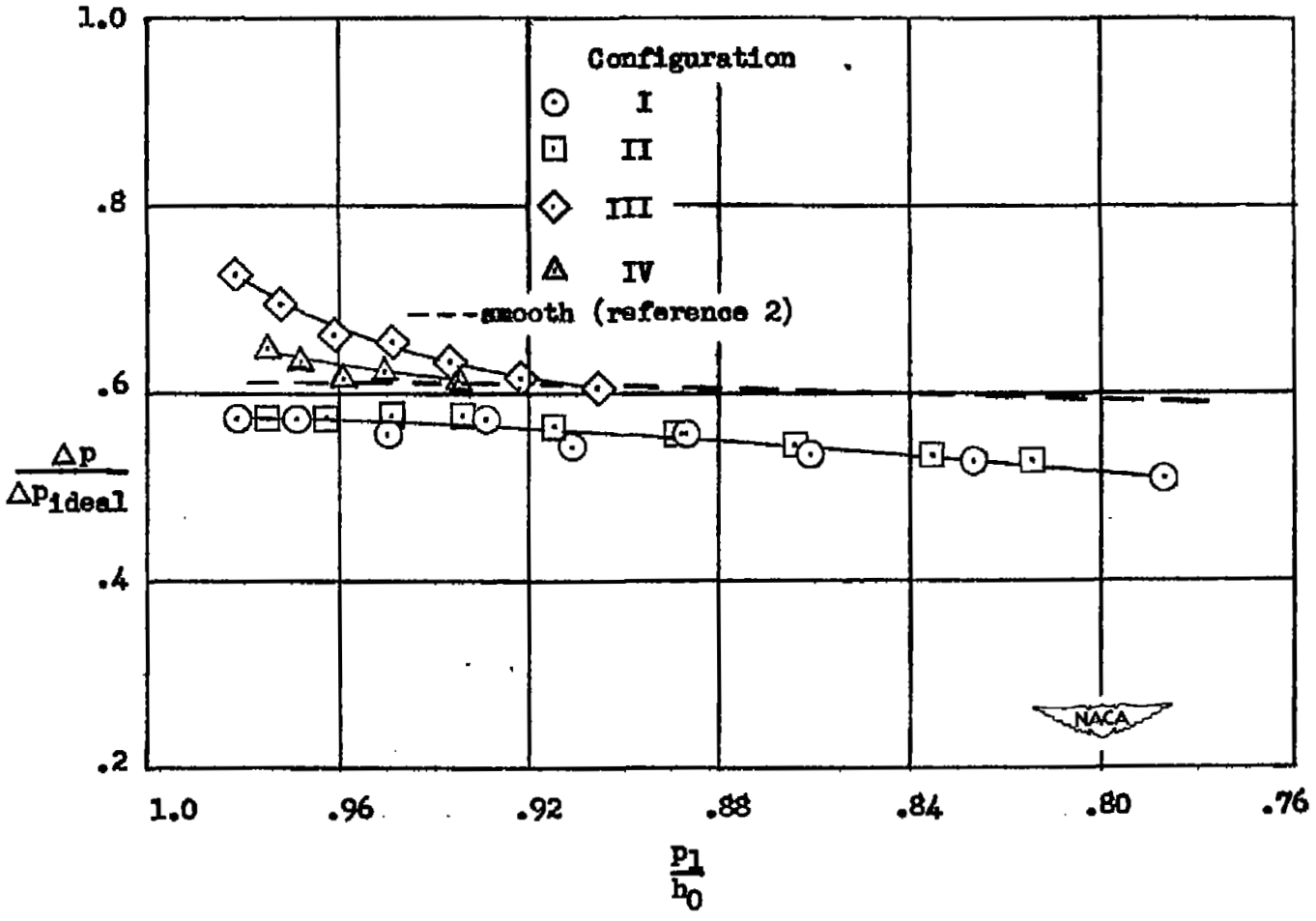

(a) Diffuser exit, station 6.

Figure 10.- Variation of diffuser effectiveness with inlet pressure ratio.

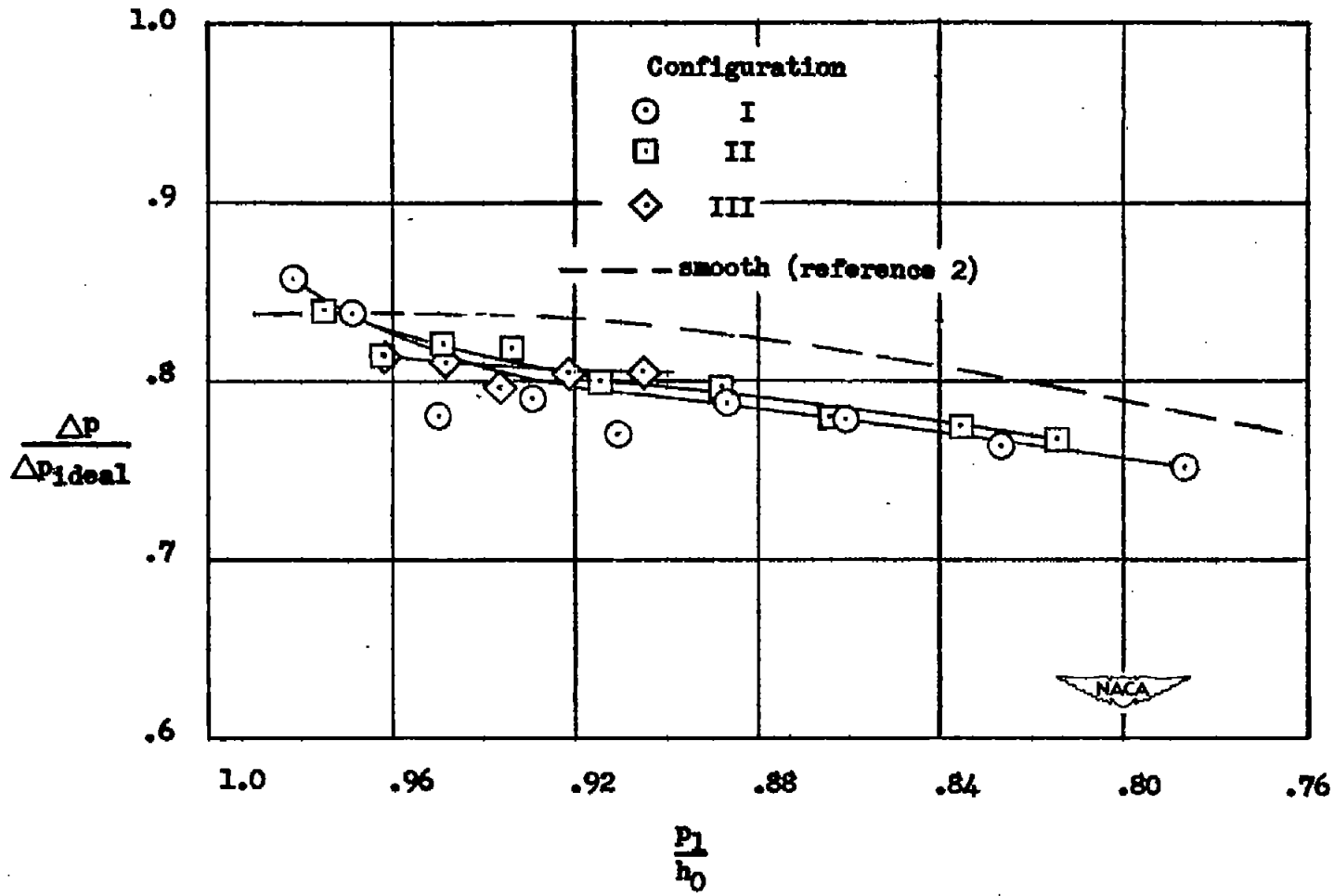

(b) Tail-pipe exit, station 7.

Figure 10.- Concluded.

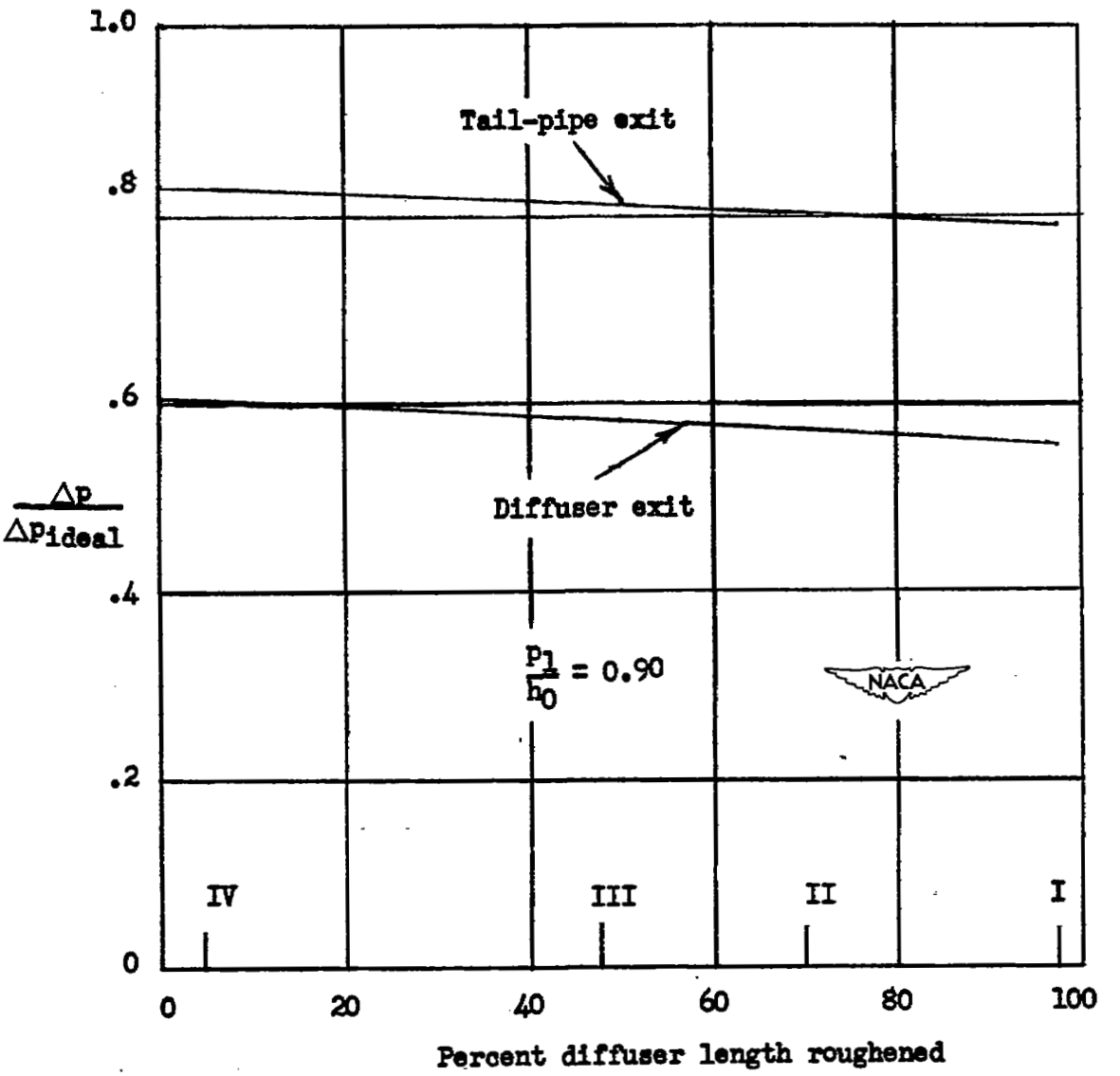

Figure 11.- Variation of diffuser effectiveness with percent of diffuser length roughened.

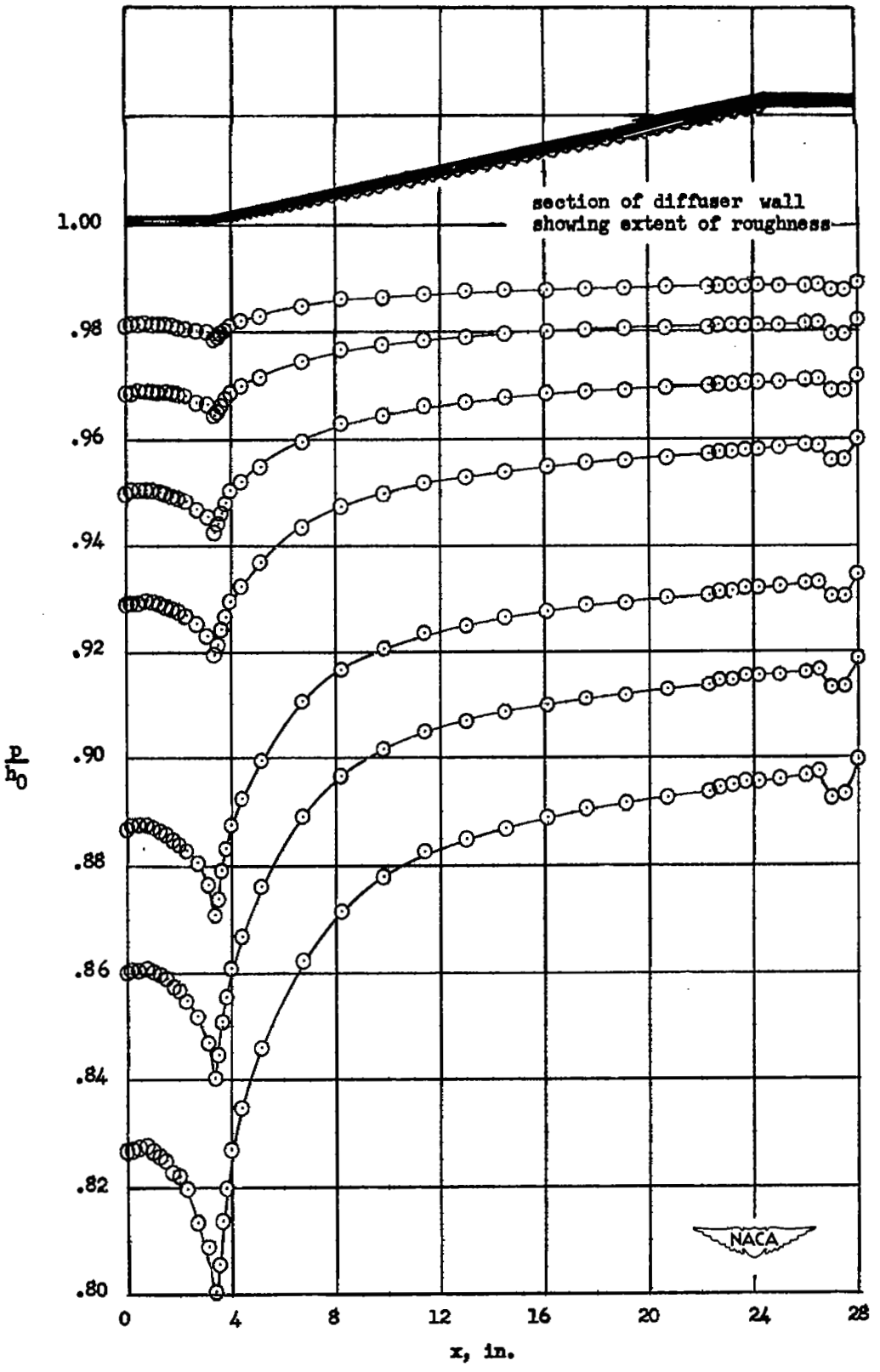

Figure 12.- Static-pressure distribution of diffuser. Configuration I.

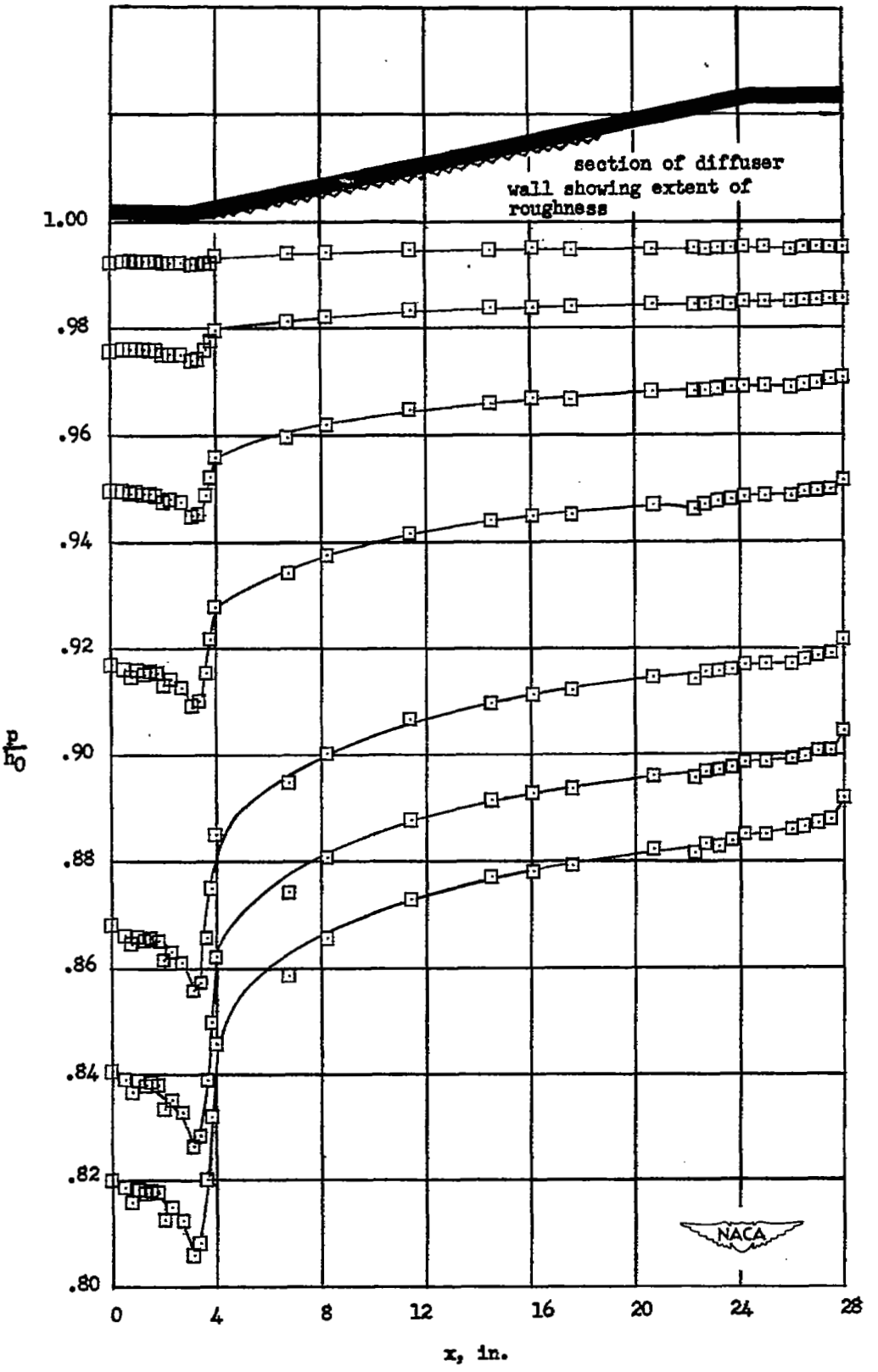

Figure 13.- Static-pressure distribution of diffuser. Configuration II.

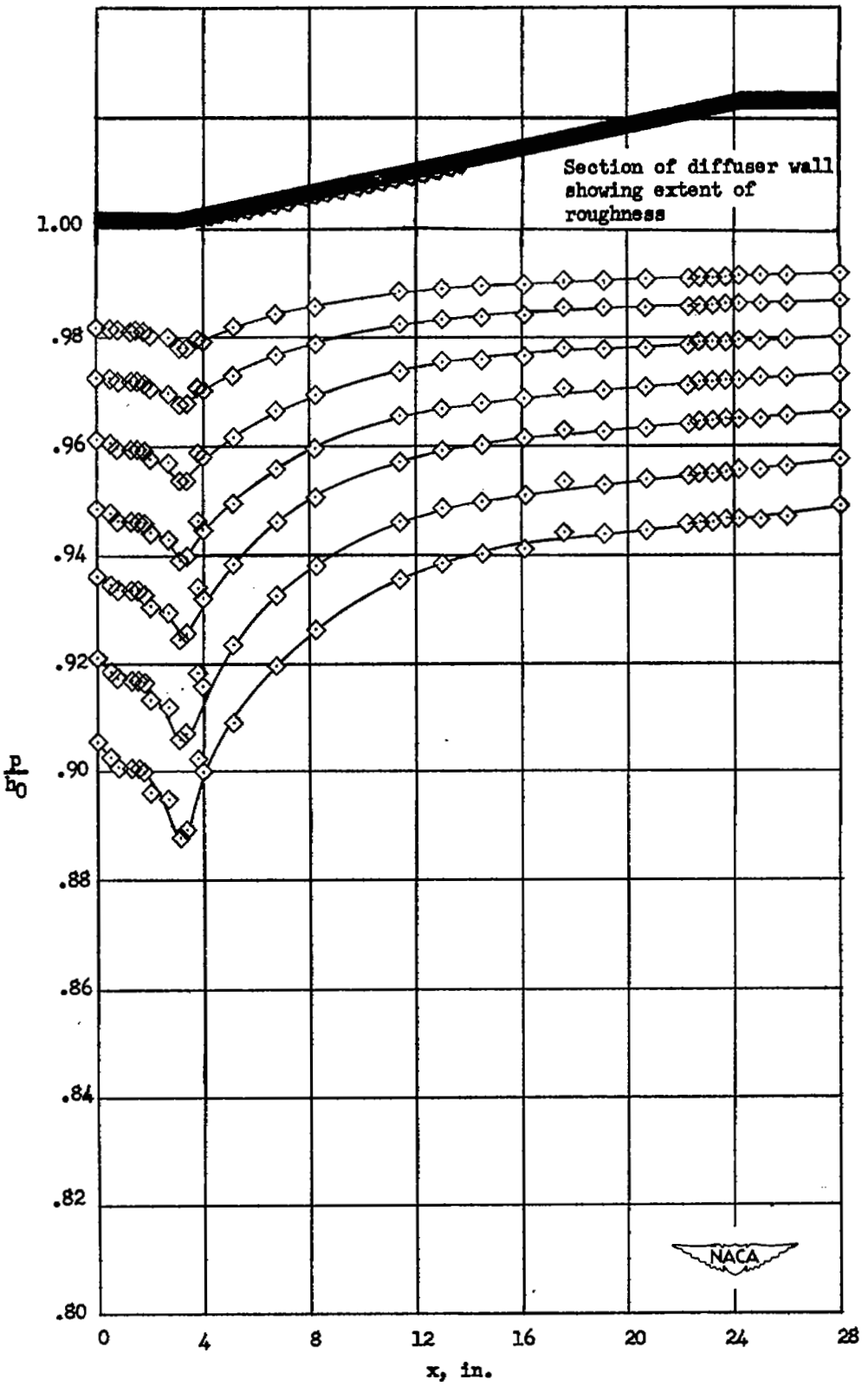

Figure 14.- Static-pressure distribution of diffuser. Configuration III.

[redacted]

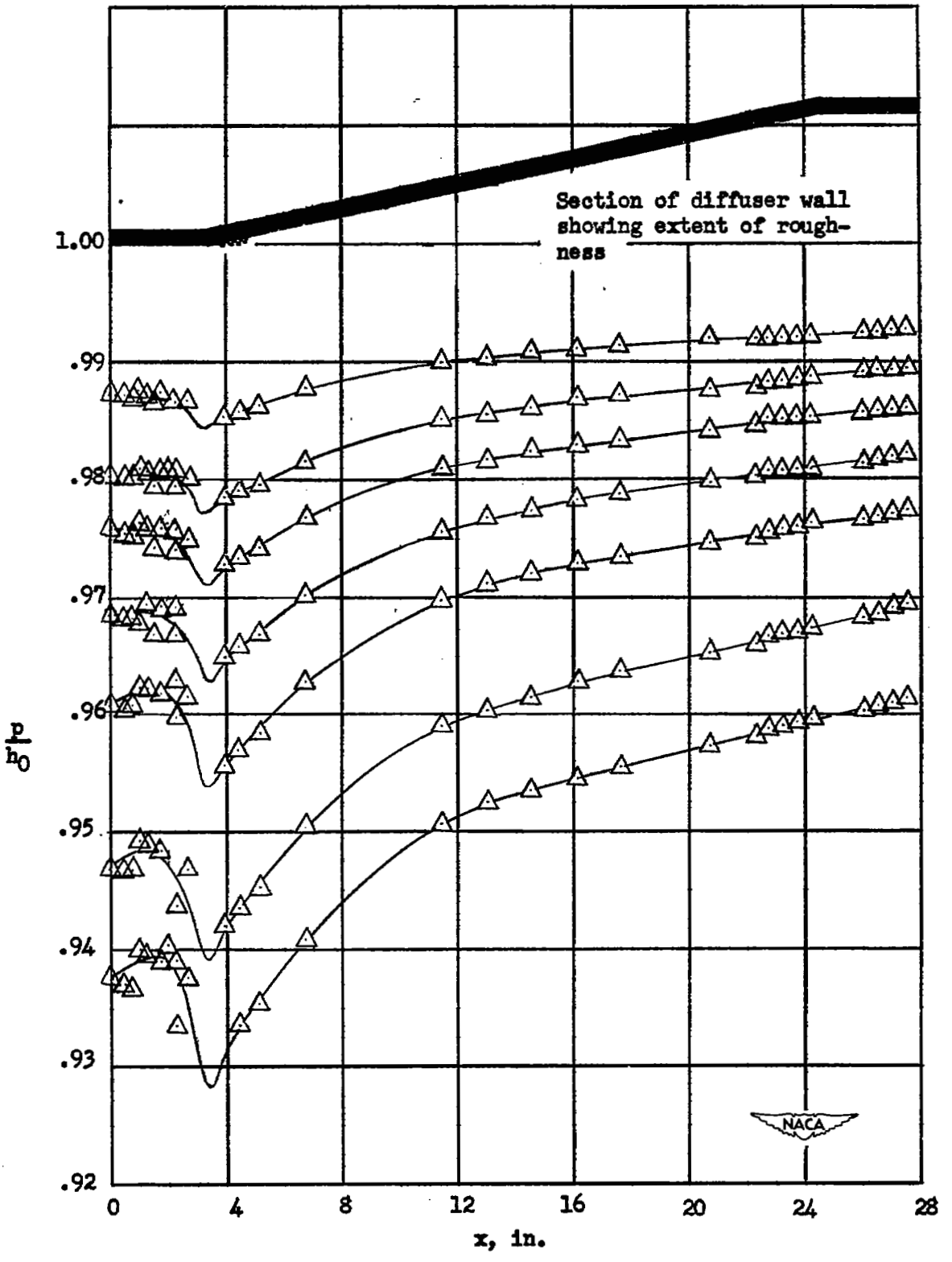

Figure 15.- Static-pressure distribution of diffuser. Configuration IV.

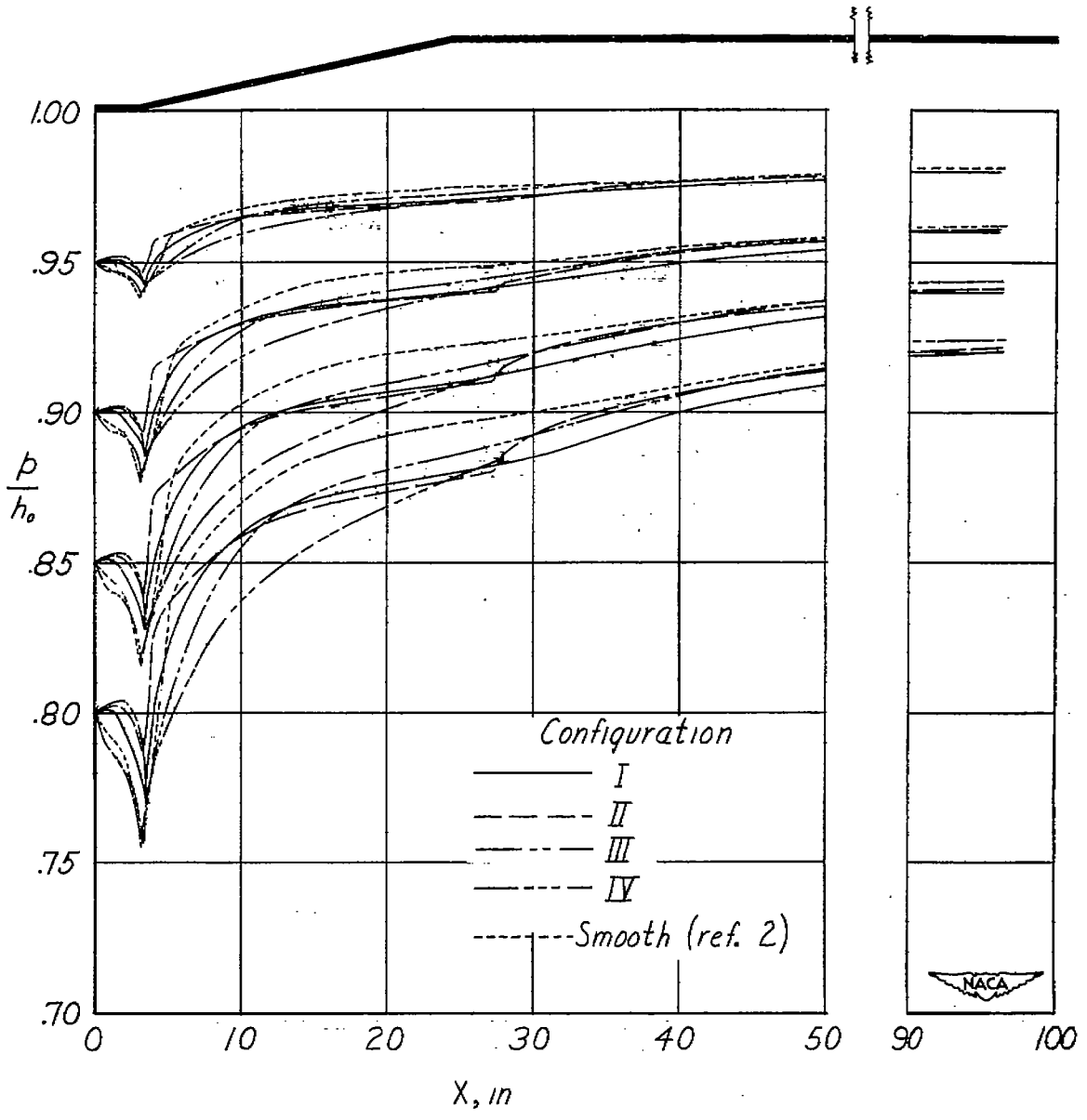

Figure 16.- Static-pressure distribution of diffuser and tail-pipe. Comparison of all configurations.

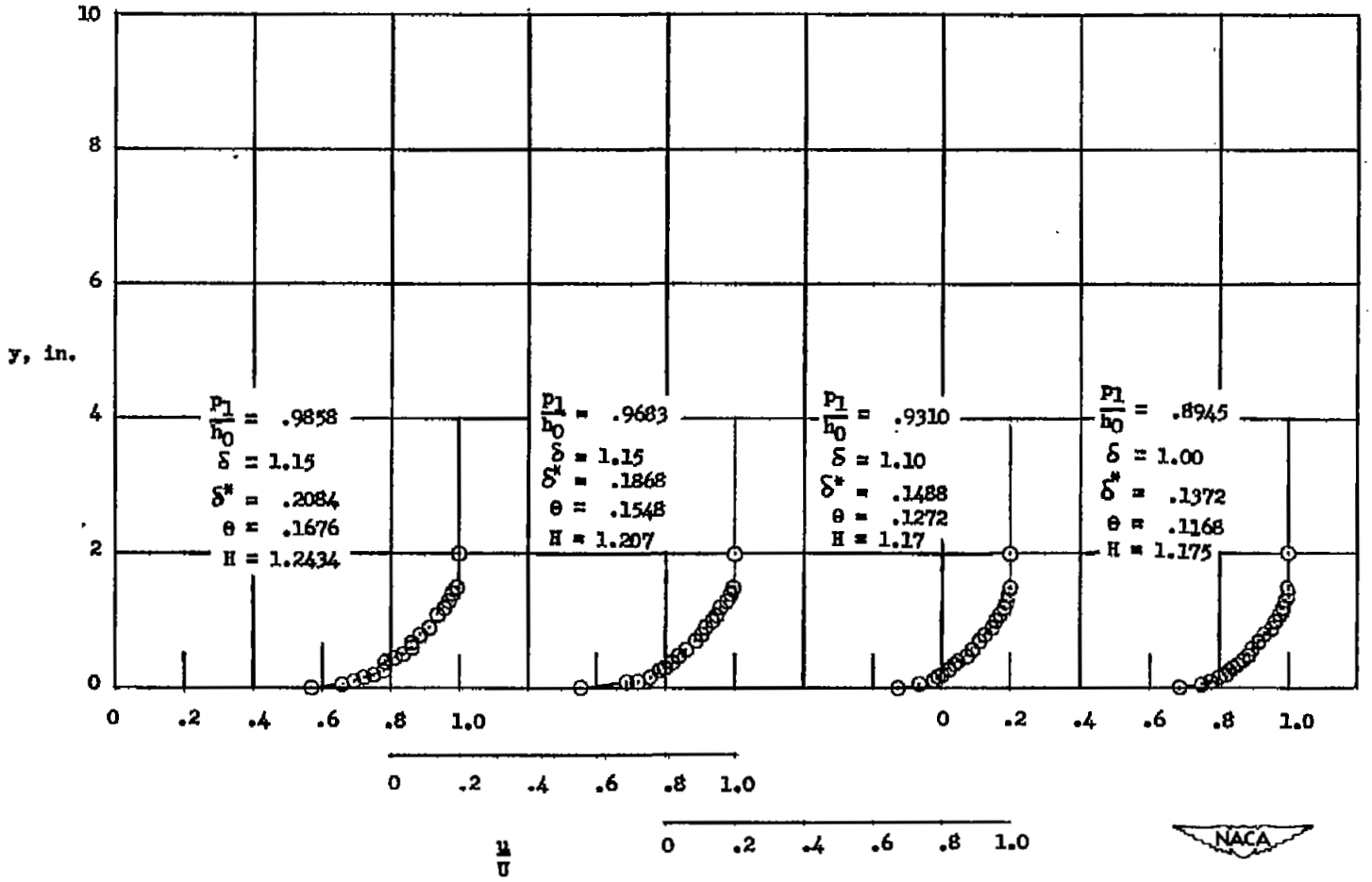

Figure 17.- Boundary-layer velocity profiles at station 1. All configurations.

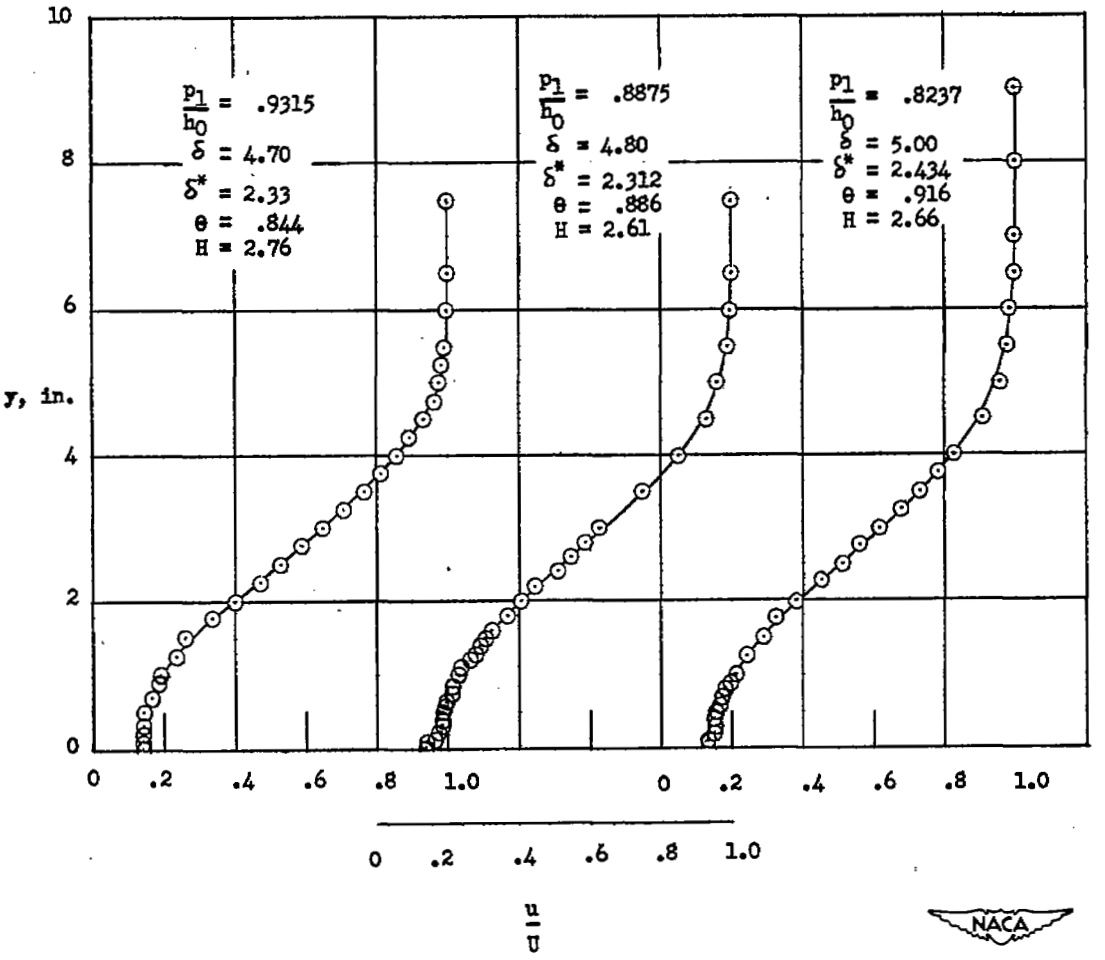

(a) Diffuser exit, station 6.

Figure 18.- Boundary-layer velocity profiles for configuration I.

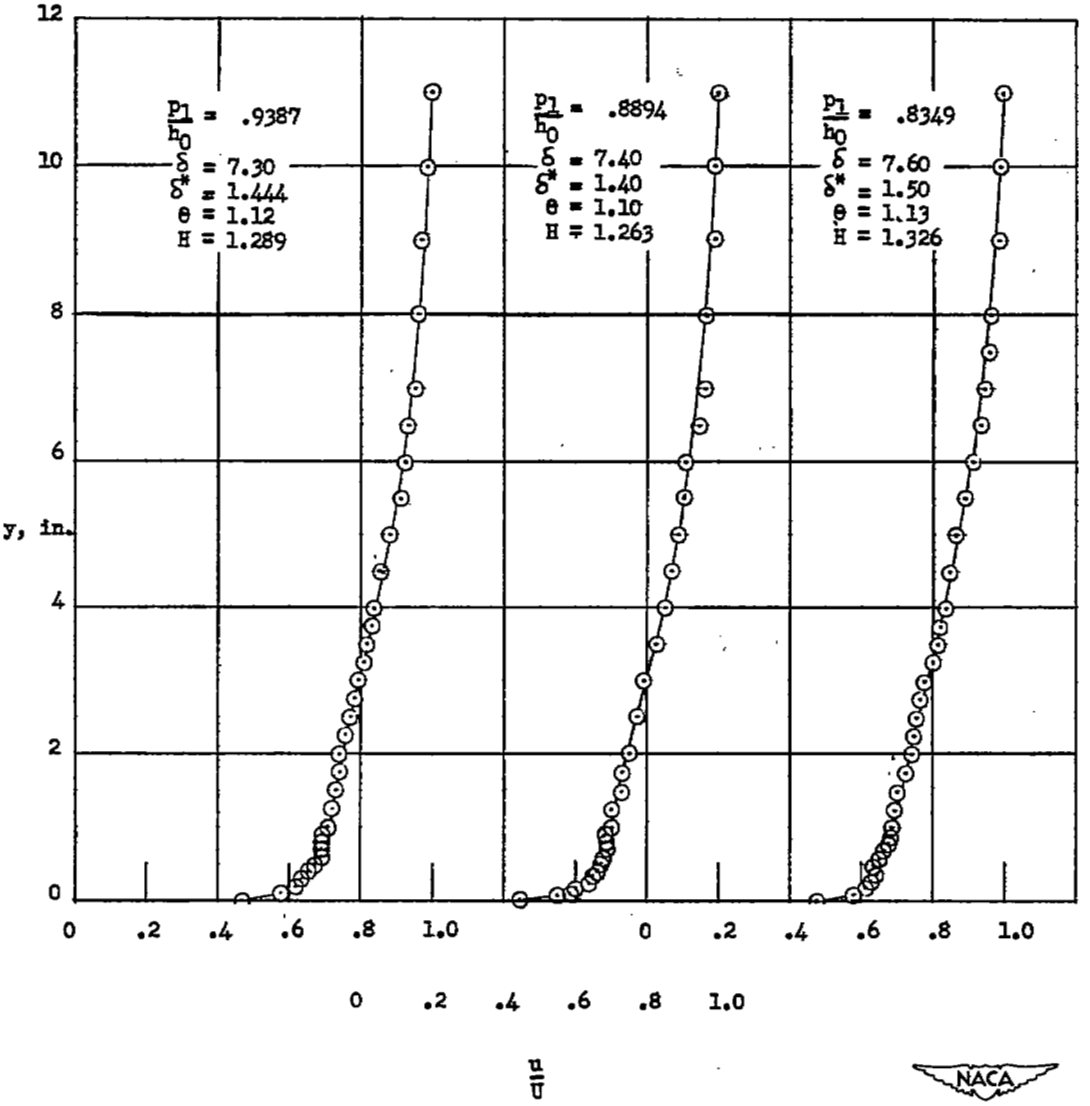

(b) Tail-pipe exit, station 7.

Figure 18.- Concluded.

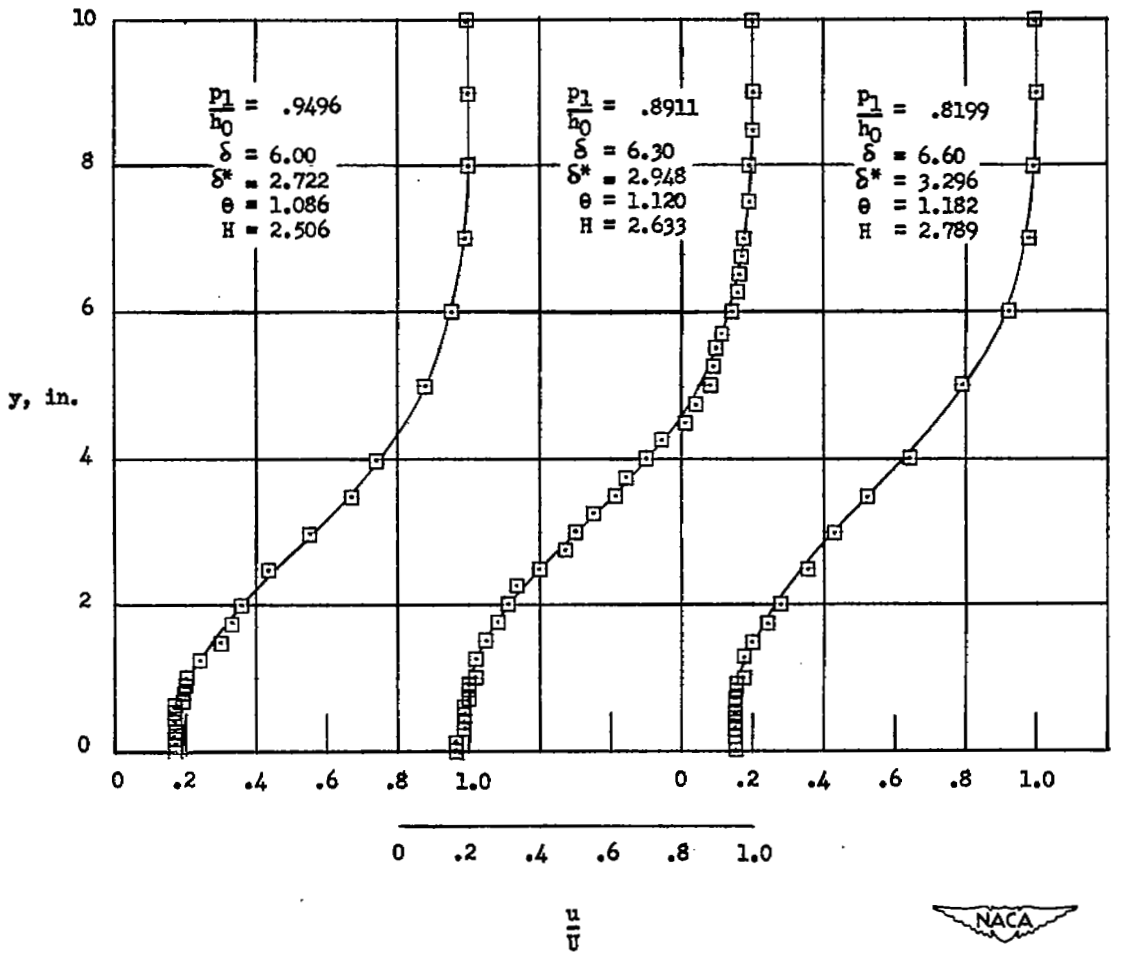

(a) Diffuser exit, station 6.

Figure 19.- Boundary-layer velocity profiles for configuration II.

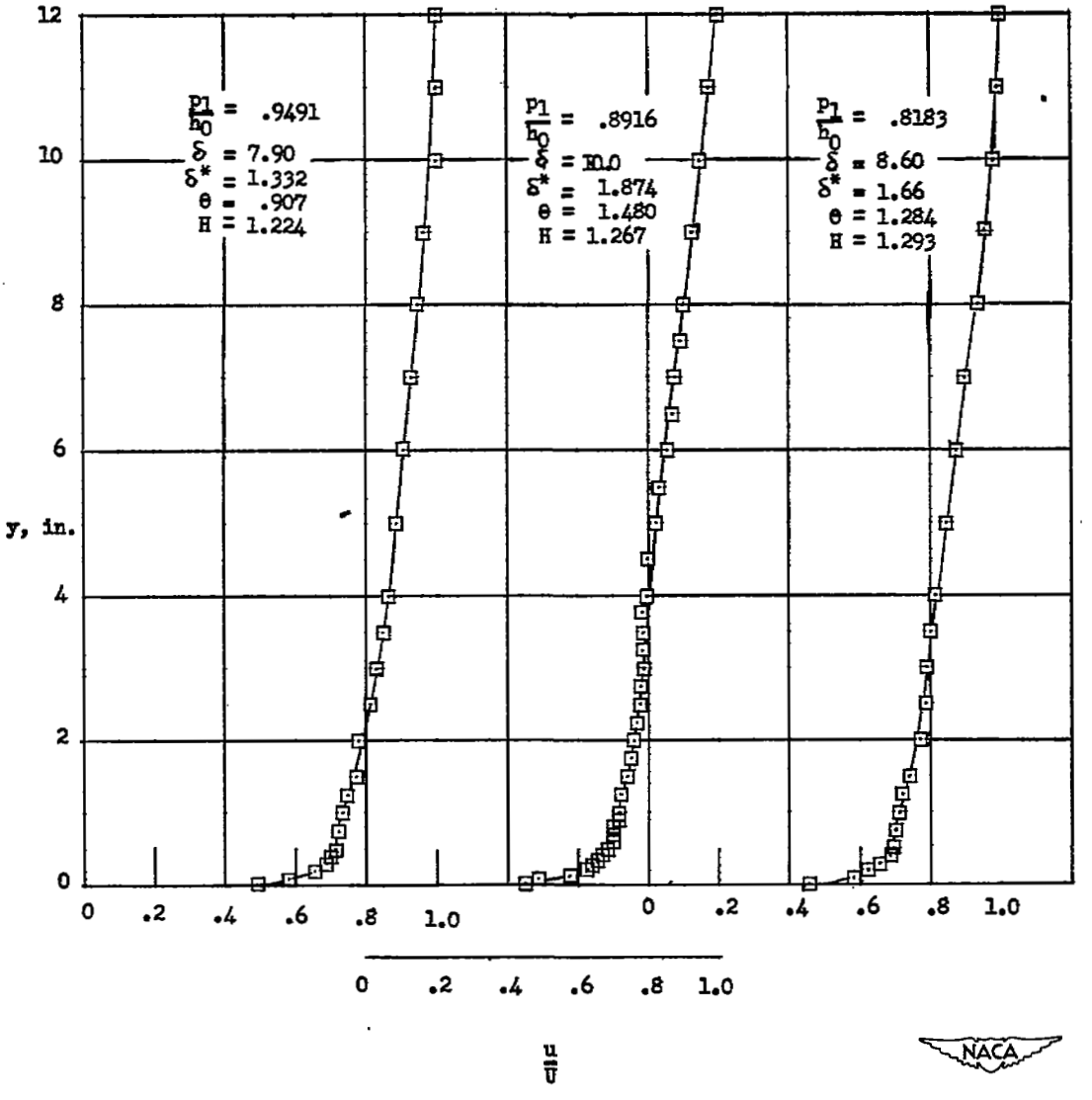

(b) Tail-pipe exit, station 7.

Figure 19.- Concluded.

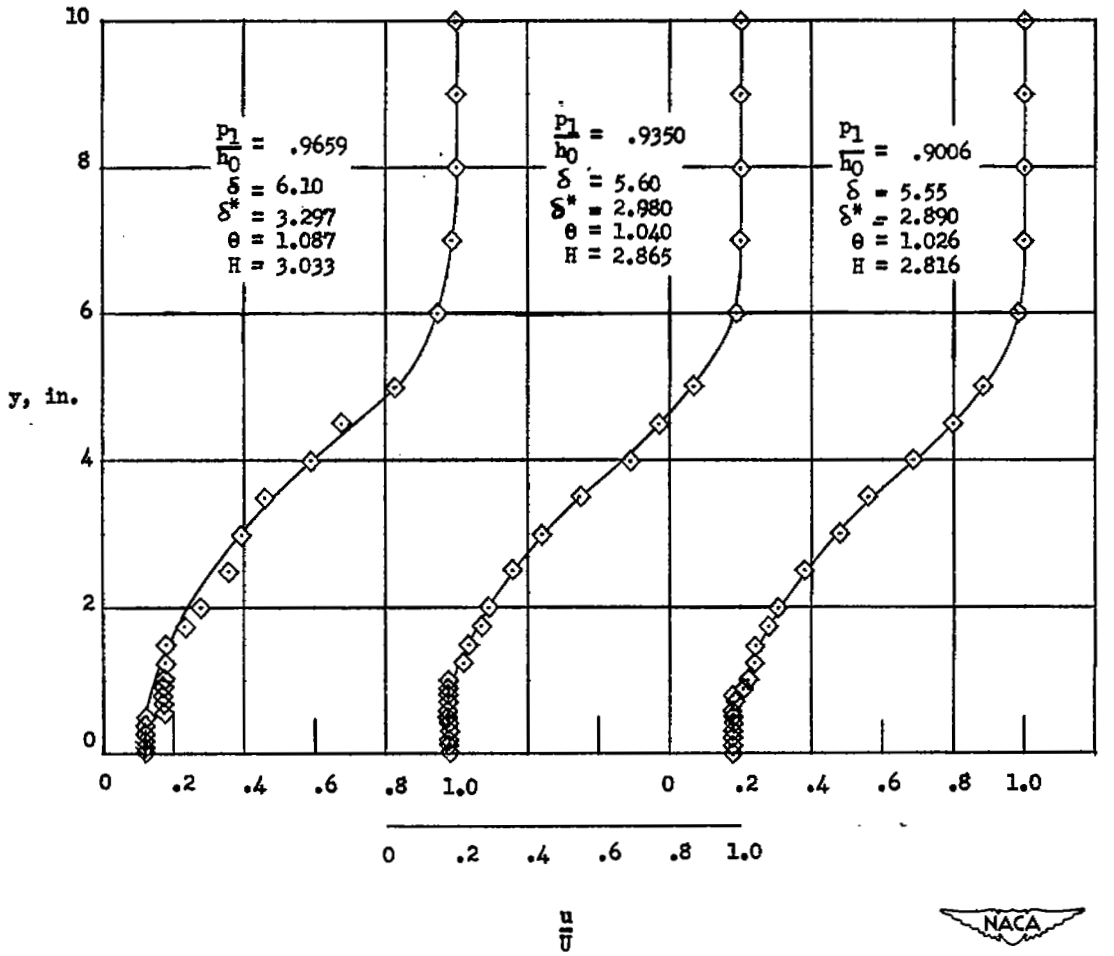

(a) Diffuser exit, station 6.

Figure 20.- Boundary-layer velocity profiles for configuration III.

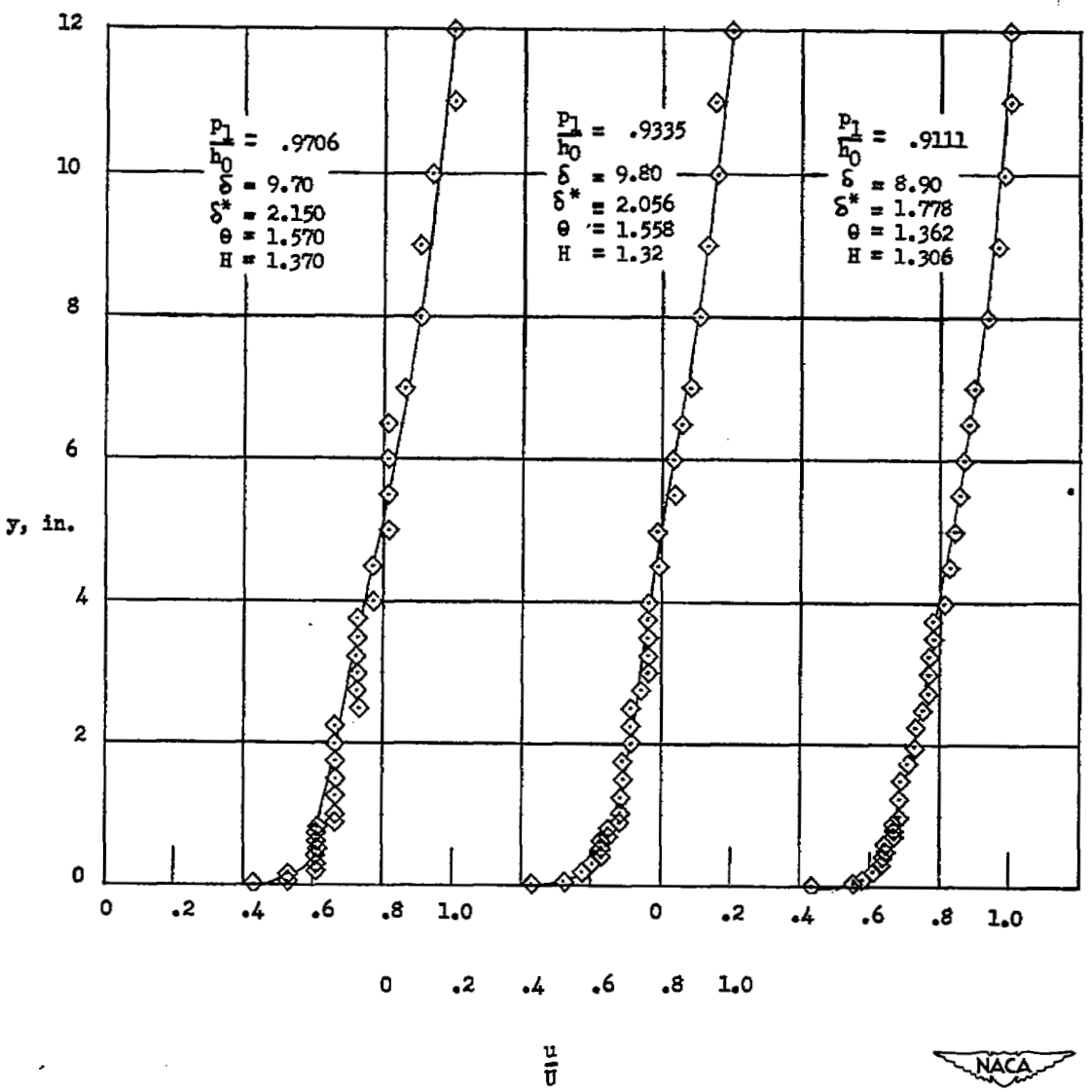

(b) Tail-pipe exit, station 7.

Figure 20.- Concluded.

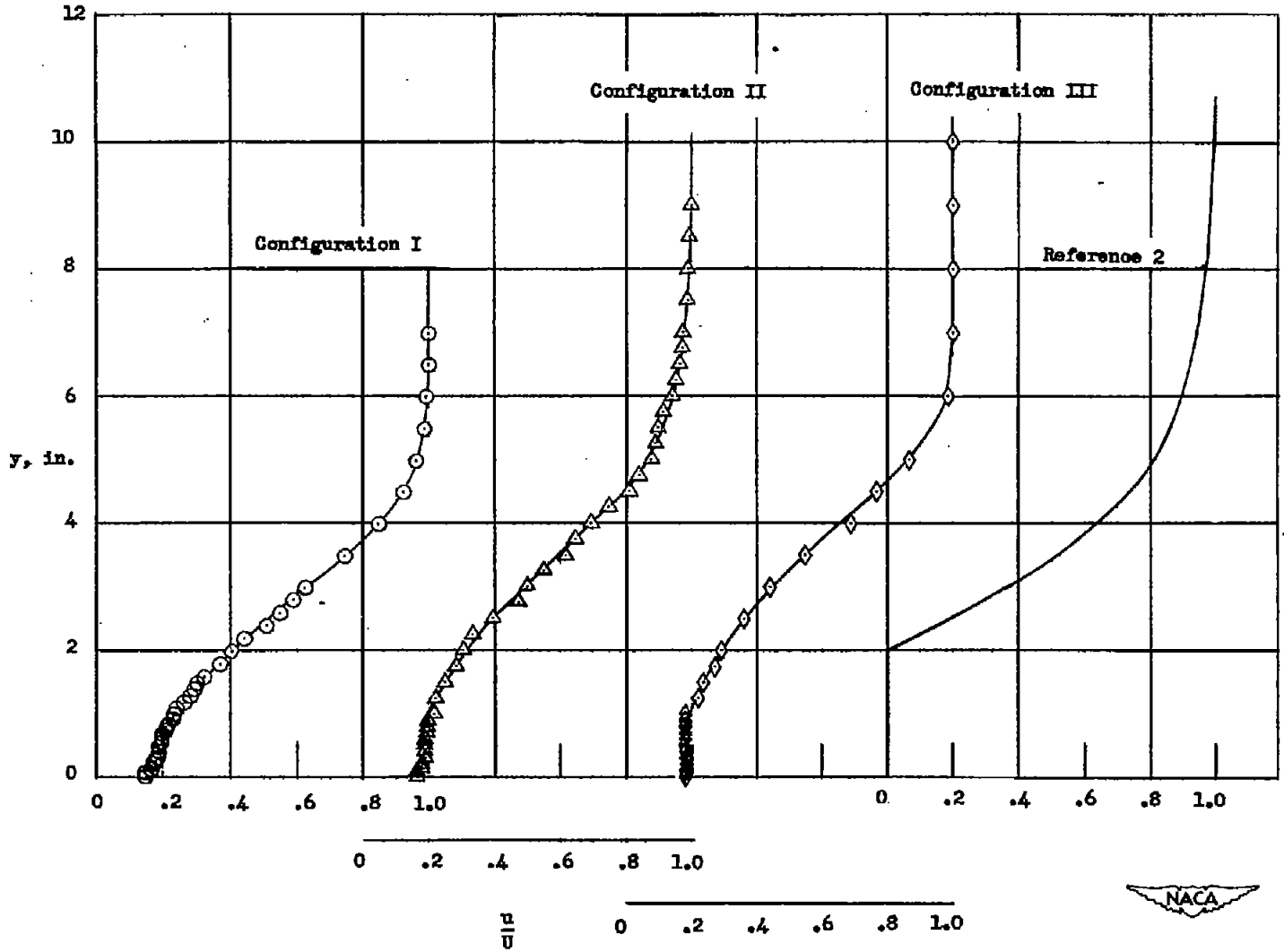

Figure 21.- Boundary-layer velocity profiles at diffuser exit, station 6. All configurations.

[redacted]